

The SCUBA HALf Degree Extragalactic Survey (SHADES) – V. Submillimetre properties of near-infrared–selected galaxies in the Subaru/*XMM*–*Newton* deep field

T. Takagi^{1,2,3*}, A.M.J. Mortier^{1,8}, K. Shimasaku⁴, K. Coppin^{5,6}, A. Pope⁵,
R. J. Ivison⁷, H. Hanami⁹, S. Serjeant¹, D.L. Clements², R. S. Priddey¹⁰,
J. S. Dunlop⁸, T. Takata¹¹, I. Aretxaga¹², S. C. Chapman¹³, S.A. Eales¹⁴,
D. Farrah¹⁵, G.L. Granato¹⁶, M. Halpern⁵, D.H. Hughes¹², E. van Kampen¹⁷,
D. Scott⁵, K. Sekiguchi¹¹, I. Smail⁶, M. Vaccari²

¹ Centre for Astrophysics and Planetary Science, University of Kent, Canterbury, Kent CT2 7NR

² Blackett Laboratory, Imperial College London, Prince Consort Road, London, SW7 2BZ

³ Institute of Space and Astronautical Science, Japan Aerospace Exploration Agency, Sagamihara, Kanagawa 229 8510, Japan

⁴ Department of Astronomy, School of Science, University of Tokyo, Tokyo 113-0033, Japan

⁵ Department of Physics & Astronomy, University of British Columbia, 6224 Agricultural Road, Vancouver, B.C., V6T 1Z1, Canada

⁶ Institute for Computational Cosmology, Durham University, South Rd, Durham, DH1 3LE

⁷ UK ATC, Royal Observatory, Blackford Hill, Edinburgh EH9 3HJ

⁸ SUPA†, Institute for Astronomy, University of Edinburgh, Royal Observatory, Edinburgh EH9 3HJ

⁹ Physics Section, Faculty of Humanities and Social Sciences, Iwate University, Morioka, 020-8550, Japan

¹⁰ Department of Physics, Astronomy & Mathematics, University of Hertfordshire, College Lane, Hatfield, Hertfordshire AL10 9AB

¹¹ Subaru Telescope, National Astronomical Observatory of Japan, 650 N. A'ohoku Place, Hilo, HI 96720, USA

¹² Instituto Nacional de Astrofísica, Óptica y Electrónica (INAOE), Apartado Postal 51 y 216, 72000 Puebla, Pue., Mexico

¹³ California Institute of Technology, 1200 East California Boulevard, Pasadena, CA 91125

¹⁴ Cardiff School of Physics and Astronomy, Cardiff University, 5, The Parade, Cardiff, CF24 3YB

¹⁵ Department of Astronomy, Cornell University, Space Sciences Building, Ithaca, NY 14853, USA

¹⁶ Istituto Nazionale di Astrofisica, Osservatorio Astronomico di Padova, Vicolo dell'Osservatorio 5, I-35100 Padova, Italy

¹⁷ Institute of Astro- and Particle Physics, University of Innsbruck, Technikerstr. 25, A-6020, Innsbruck, Austria

ABSTRACT

We have studied the submillimetre (submm) properties of the following classes of near-infrared (NIR)-selected massive galaxies at high redshifts: *BzK*-selected star-forming galaxies (*BzK*s); distant red galaxies (DRGs); and extremely red objects (EROs). We used the SCUBA HALf Degree Extragalactic Survey (SHADES), the largest uniform submm survey to date. Partial overlap of SIRIUS/NIR images and SHADES in SXDF has allowed us to identify 4 submm-bright NIR-selected galaxies, which are detected in the mid-infrared, 24 μm , and the radio, 1.4 GHz. We find that all of our submm-bright NIR-selected galaxies satisfy the *BzK* selection criteria, i.e. $BzK \equiv (z - K)_{\text{AB}} - (B - z)_{\text{AB}} \geq -0.2$, except for one galaxy whose $B - z$ and $z - K$ colours are however close to the *BzK* colour boundary. Two of the submm-bright NIR-selected galaxies satisfy all of the selection criteria we considered, i.e. they belong to the *BzK*-DRG-ERO overlapping population, or ‘extremely red’ *BzK*s. Although these extremely red *BzK*s are rare (0.25 arcmin⁻²), up to 20% of this population could be submm galaxies. This fraction is significantly higher than that found for other galaxy populations studied here. Via a stacking analysis, we have detected the 850- μm flux of submm-faint *BzK*s and EROs in our SCUBA maps. While the contribution of $z \sim 2$ *BzK*s to the submm background is about 10–15% and similar to that from EROs typically at $z \sim 1$, *BzK*s have a higher fraction ($\sim 30\%$) of submm flux in resolved sources compared with EROs and submm sources as a whole. From the SED fitting analysis for both submm-bright and submm-faint *BzK*s, we found no clear signature that submm-bright *BzK*s are experiencing a specifically luminous evolutionary phase, compared with submm-faint *BzK*s. An alternative explanation might be that submm-bright *BzK*s are more massive than submm-faint ones.

Key words: galaxies: starburst – dust, extinction – infrared: galaxies – submillimetre

1 INTRODUCTION

The first 3–4 billion years in the history of the universe appears to have been a very important epoch for the formation of present-day massive galaxies, in particular for elliptical galaxies and bulges with masses of $M \gtrsim 10^{11} M_{\odot}$. Recent wide field near-infrared (NIR) surveys in conjunction with multi-band optical images or spectroscopy have resulted in a profusion of samples of massive galaxies at high redshifts (e.g. Franx et al. 2003; Fontana et al. 2003; Dickinson et al. 2003; Fontana et al. 2004; Cimatti et al. 2004; Glazebrook et al. 2004; Daddi et al. 2004; Juneau et al. 2005; Labbé et al. 2005; Drory et al. 2005; Reddy et al. 2005; Kong et al. 2006; Papovich et al. 2006; Daddi et al. 2007; Arnouts et al. 2007; Pozzetti et al. 2007). At $z \sim 2$, the physical properties of massive galaxies are very different from those of present-day ones, i.e. a large fraction of them are intensively star-forming galaxies (e.g. Daddi et al. 2005), rather than passively evolving, like nearby ones. A notable characteristic of these massive star-forming galaxies is that, in some cases, a large total stellar mass $\sim 10^{11} M_{\odot}$ could be formed in the time-scale of a single starburst event, ~ 0.1 Gyr (Pérez-González et al. 2005; Caputi et al. 2006; Papovich et al. 2006).

Massive, intensively star-forming galaxies have also been found in submillimetre (submm) surveys (Smail et al. 1997; Hughes et al. 1998; Eales et al. 1999; Scott et al. 2002; Borys et al. 2003; Mortier et al. 2005; Coppin et al. 2006). These submm galaxies turn out to be typically starbursts or starburst/AGN composite systems at $z \sim 2$ (Chapman et al. 2005; Alexander et al. 2005, and references therein), which are massive (Swinbank et al. 2004; Greve et al. 2005). They are likely to become passively evolving massive galaxies at lower redshifts (e.g. Smail et al. 2004; Blain et al. 2004; Takagi et al. 2004). The star formation rates (SFRs) of submm-bright galaxies are estimated to be extraordinarily high, $\sim 10^3 M_{\odot} \text{ yr}^{-1}$ (e.g. Greve et al. 2005; Alexander et al. 2005; Chapman et al. 2005; Pope et al. 2006; Kovács et al. 2006), enough to produce a massive elliptical galaxy ($> 3 L^*$) within ~ 1 Gyr. Determining the nature of these star-forming galaxies at high redshifts may be the key to understanding the process of massive galaxy formation.

Efficient methods for selecting massive star-forming galaxies at high redshifts with one or two optical/NIR colours have played a significant role in studying the properties of massive galaxy populations. These include *BzK*-selected galaxies (selected in $B - z$ and $z - K$ colours), distant red galaxies (selected with $J - K$ colour), and extremely red objects (selected with $R - K$ or $I - K$ colour). Hereafter we call these galaxy populations NIR-selected galaxies or NIRGs.

Daddi et al. (2004) proposed an effective method for selecting massive star-forming galaxies at $1.4 \lesssim z \lesssim 2.5$ along with the selection of passively evolving galaxies at a similar redshift range in a colour-colour diagram of $B - z$ vs $z - K$. It is expected to be reddening independent, i.e. applicable to heavily obscured galaxies like ultraluminous infrared galaxies (ULIRGs). Their luminosities at UV (reddening corrected), infrared, X-ray and radio indicate that *BzK*-selected star-forming galaxies (*BzKs*)¹ with $K < 20$

are typically ULIRGs with SFRs of $\sim 200 M_{\odot} \text{ yr}^{-1}$ and reddening of $E(B - V) \sim 0.4$ (Daddi et al. 2004, 2005; Reddy et al. 2005; Kong et al. 2006).

In an alternative approach, Franx et al. (2003) employed a colour cut of $(J - K_s)_{\text{vega}} > 2.3$ to select distant red galaxies (DRGs). This colour criterion selects both passively evolving and heavily obscured star-forming galaxies at $2 < z < 4.5$ with strong Balmer or 4000Å breaks. Recent *Spitzer* imaging at $24 \mu\text{m}$ suggests that the bulk of DRGs are dusty star-forming galaxies (Webb et al. 2006; Papovich et al. 2006). Similar to *BzK*-selected star-forming galaxies, DRGs are likely to be ULIRGs at $z \sim 2$ (e.g. Knudsen et al. 2005), but to also include a significant fraction of less luminous dusty star-forming galaxies at $1 < z < 2$ (Grazian et al. 2006). Submm galaxies, another sample of ULIRGs at $z \sim 2$, could have a large overlap with *BzKs* or DRGs, but with systematically higher SFR than the average (e.g. Dannerbauer et al. 2006).

Extremely red objects (EROs) defined with $R - K$ or $I - K$ colours have received particular attention as possible optical-NIR counterparts of submm galaxies (e.g. Smail et al. 1999; Webb et al. 2003; Pope et al. 2005), since submm galaxies are expected to be heavily obscured by dust and therefore red. However, it turns out that only 10–30% of submm galaxies, whose optical counterparts are identified with associated radio sources, are EROs (Ivison et al. 2002; Webb et al. 2003; Borys et al. 2004; Smail et al. 2004). The median redshift of EROs with $K_{\text{vega}} < 19.2$ is $z = 1.1 \pm 0.2$ (Cimatti et al. 2002), and therefore lower than that of resolved submm-bright galaxies, *BzKs* and DRGs. Nevertheless, there is certainly some overlap between their redshift distributions.

It is important to understand the physical relationships between these high- z massive star-forming galaxies which are selected in different ways (e.g. see Reddy et al. 2005). The surface density of *BzKs*, DRGs and EROs is similar to each other, about $1\text{--}2 \text{ arcmin}^{-2}$ with $K_{\text{vega}} \lesssim 20$ (Daddi et al. 2004; Cimatti et al. 2002; van Dokkum et al. 2003). A similar surface density has been found for submm galaxies with $S_{850\mu\text{m}} \gtrsim 1 \text{ mJy}$ (e.g. Blain et al. 1999), although the surface density of bright ($S_{850\mu\text{m}} \gtrsim 8 \text{ mJy}$) submm galaxies in ‘blank sky’ surveys is at least an order of magnitude smaller. Understanding the physical origin of the overlap between submm galaxies and NIR-selected galaxies is not straightforward, given the diverse optical-NIR properties of submm galaxies, which include those similar to less-attenuated UV-selected galaxies as well as EROs (e.g. Smail et al. 2002, 2004).

Here we study the submm properties of *BzKs*, DRGs and EROs by using the SCUBA Half Degree Extragalactic Survey (SHADES – Mortier et al. 2005), providing a larger sample of submm galaxies for investigating the relation between submm galaxies and NIRGs than the study of Reddy et al. (2005) for galaxies in the GOODS-North field. SHADES has mapped two regions in the Lockman Hole and in the Subaru/*XMM-Newton* deep field (SXDF). In this study, we focus on a 93 arcmin^2 sub-region of the

selected galaxies and submm galaxies, star-forming galaxies selected with this method are simply referred to as *BzK*-selected galaxies or *BzKs*.

¹ Since we are studying cross-identifications between *BzK*-

SXDF field of SHADES, in which both optical ($BVRi'z'$) and NIR (JHK_s) photometry are already available. We describe the data in Section 2 and the sample of NIR-selected galaxies in Section 3. In Section 4, we identify submm-bright NIR-selected galaxies and assess the overlap between submm galaxies and NIR-selected galaxies. In Section 5, we present the results of a statistical detection of NIR-selected galaxies in the SCUBA map using a stacking analysis. In Section 6, we analyse the spectral energy distributions (SEDs) of submm-bright NIR-selected galaxies and also an average SED of submm-faint NIRGs, in order to investigate their physical properties. Summary of our study is given in Section 7. Throughout this paper, we adopt the cosmology of $\Omega_m = 0.3$, $\Omega_\Lambda = 0.7$ and $H_0 = 70 \text{ km sec}^{-1} \text{ Mpc}^{-1}$. All the magnitudes are given in the AB system, unless otherwise noted.

2 THE DATA

2.1 Optical/NIR data in the SXDF

We have used the optical and NIR imaging data of the SXDF centred at $[2^{\text{h}}18^{\text{m}}00^{\text{s}}, -5^{\circ}00'00'' \text{ (J2000)}]$ published by Miyazaki et al. (2003). The NIR data were obtained with the University of Hawaii 2.2 m telescope with the Simultaneous 3-colour InfraRed Imager for Unbiased Survey (SIRIUS; Nagayama et al. 2003). The final image covers an area of 114 arcmin^2 in the H - and K_s -bands. For the J -band, we obtained data only for 77 arcmin^2 , since a quarter of the field of view was not operational. The 5σ detection limits of the final NIR image are $J = 22.8$, $H = 22.5$ and $K_s = 22.1$ mag, through a $2''$ diameter aperture. From the final image in the K_s -band, we have detected 1308 objects having $K_s < 22.1$ mag using SExtractor (Bertin & Arnouts 1996). Throughout this work we use the total magnitudes in the optical-NIR bands measured with the MAG_AUTO algorithm in SExtractor.

For these K_s -band detected objects, we made a multi-band catalogue using optical images of Subaru/Suprime-cam (Miyazaki et al. 2002) in B , V , R , i' , z' bands². The limiting magnitudes (5σ) of our images are $B = 27.1$, $V = 25.9$, $R = 26.3$, $i' = 25.7$, $z' = 25.0$ mag through a $2''$ diameter aperture. The FWHM of the point-spread function is $0.98''$ in both the optical and NIR images. Stars were identified with the colour criterion of $B - K_s < 1.583(B - i') - 0.5$ and $\text{FWHM} \leq 1.2''$ (Miyazaki et al. 2003), and removed from the analysis.

2.2 Submm/radio data from SHADES

Details of the survey design and observing strategy with JCMT/SCUBA are given in Mortier et al. (2005). Here we describe the SHADES survey only briefly. Using the SCUBA instrument on the JCMT we have obtained jiggle maps of the SXDF and also the Lockman Hole in grade 2–3 weather ($\tau_{\text{CSO}} = 0.05 - 0.1$). The FWHM of the SCUBA beam is $14.7''$ and $7.8''$ at 850 and 450 μm , respectively. The SHADES observations with SCUBA were continued from

December 2002 to the decommissioning of SCUBA in June 2005. Here we use the SCUBA data acquired until 1st Feb, 2004.

The SCUBA data have been reduced by four independent groups in the SHADES consortium. Practical methods of data reduction, such as flux calibration, extinction correction, and map making depends on the reduction group and are summarised in Coppin et al. (2006). The extracted sources from four different SCUBA maps have been compared and then combined to produce the SHADES source catalogue, which is expected to be the most reliable source catalogue from SCUBA surveys. In our analyses, we focus on two particular SCUBA maps out of four, along with the SHADES source catalogue, in order to make the sample of submm-bright NIRGs as complete as possible.

We have chosen to use only regions with noise less than 3 mJy at 850 μm . The total area of this region is $\sim 250 \text{ arcmin}^2$. The field centre for the SHADES map of the SXDF, $02^{\text{h}}17^{\text{m}}57^{\text{s}}.5$, $-05^{\circ}00'18''.5$ (J2000), is offset from that of the SIRIUS observations and hence our sub-mm maps do not cover the whole region covered by the NIR data. In one of the four SCUBA maps ('Reduction B' in Coppin et al.), this overlap is 93 arcmin^2 , with median noise levels of 2.0 mJy and 18.4 mJy at 850 and 450 μm , respectively.

Wide-field 1.4-GHz radio images of SXDF were obtained using the VLA during 2003. Around 60 hr of integration were salvaged, following a prolonged failure of the correlator, comprising data from the A, B and C configurations, with an approximate 9:3:1 ratio of recorded visibilities, evenly distributed in three pointings separated by 15 arcmin. The final images were mosaiced together, after correcting for the response of the primary beam. The resulting noise level is around $7 \mu\text{Jy beam}^{-1}$ in the best regions of the map (rather higher near bright, complex radio emitters) with a synthesised beam measuring $1.87 \times 1.65 \text{ arcsec}$ (FWHM), major axis 22° east of north. The data and their reduction are described in detail in Ivison et al. (2007).

2.3 Spitzer data from SWIRE

The whole area of our K_s -band image is covered by the Spitzer Wide-area InfraRed Extragalactic survey (SWIRE; Lonsdale et al. 2003). We used the IRAC+24 μm catalogue from version 2.0 data products (released in Summer 2005), available from the NASA/IPAC Infrared Service Archive (IRSA). We adopted the Kron fluxes, which are MAG_AUTO fluxes from SExtractor, in order to compare with the ground-based optical-NIR photometry. This catalogue includes IRAC sources which are detected at both 3.6 μm ($> 10\sigma$) and 4.5 μm ($> 5\sigma$). The astrometric error of the IRAC sources is small enough to easily identify counterparts of NIRGs with the angular separation of $\lesssim 0.5''$. In the SIRIUS/ K_s -band region, the faintest sources at 24 μm in the catalogue have a flux of $\sim 300 \mu\text{Jy}$. Cross-correlation between the SHADES sources and the SWIRE sources in SXDF is given in Clements et al. (2007, in preparation).

² Our data were obtained during the commissioning phase of the Suprime-cam.

3 SAMPLE OF NIR-SELECTED GALAXIES AT HIGH REDSHIFTS

3.1 EROs and DRGs

Following Miyazaki et al. (2003), we define EROs as objects with $R - K_s > 3.35$, which is equivalent to $(R - K)_{\text{Vega}} \gtrsim 5$, i.e. the widely used criterion of EROs. In order to obtain the DRG sample, we use the threshold of $J - K_s > 1.32$ (i.e. $\gtrsim 2.3$ in Vega magnitudes). Within the SHADES area, we have detected 201 EROs and 67 DRGs in total, among which 39 objects satisfy both $R - K_s > 3.35$ and $J - K_s > 1.32$. In Figure 1, we show a colour-colour plot with $R - K_s$ and $J - K_s$ for K_s -band detected objects, along with the adopted colour criteria. The statistics of NIRGs are summarised in Table 1.

We derived a surface density of 2.18 ± 0.14 and $1.09 \pm 0.12 \text{ arcmin}^{-2}$ (Poissonian errors) for EROs and DRGs, respectively. By using the same data, Miyazaki et al. (2003) found a good agreement in the surface density of EROs with those of the other surveys with areas of $> 50 \text{ arcmin}^2$ (Cimatti et al. 2002; Daddi et al. 2000; Thompson et al. 1999). The surface density of DRGs is coincidentally very similar to that derived by van Dokkum et al. (2003), although the K_s -band limiting magnitude in van Dokkum et al. (2003) is ~ 0.7 mag deeper than ours. Thus, we find a higher surface density of $K_s \lesssim 20$ DRGs than in van Dokkum et al. (2003). This could be partly because of the contamination of the sample at $K_s > 21.5$ where the detection of DRGs at J -band is possible only below 4σ .

3.2 BzK-selected star-forming galaxies

Daddi et al. (2004) proposed a joint selection of star-forming galaxies and passively evolving galaxies in the redshift range of $z = 1.4\text{--}2.5$ in the $z - K$ vs $B - z$ diagram (hereafter ‘ BzK diagram’). Following Daddi et al. (2004), we choose BzK -selected galaxies with $BzK \geq -0.2$, where $BzK \equiv (z - K) - (B - z)$. In order to adjust the selection in our photometric bands to that of Daddi et al., we compared the stellar sequence in the BzK diagram with that of Daddi et al. (2004). To match the stellar sequence, we applied the following colour corrections: $(B - z)_{\text{Daddi}} = (B - z') + 0.2$ and $(z - K)_{\text{Daddi}} = (z' - K) - 0.2$. After this correction, we obtained 132 BzK -selected galaxies within the SHADES area.

We obtained a surface density of 1.1 arcmin^{-2} for $K_s < 20$ (Vega). This surface density is consistent with that of Daddi et al. (2005), who found 169 BzK s within 154 arcmin^2 , including X-ray detected objects, in the GOODS North region. Thus, we assume there are no systematic differences between our sample and that of Daddi et al. (2005). In Figure 2, we plot the raw BzK colour (i.e. with no colour corrections) of K_s -band detected objects against K_s magnitudes along with the photometric errors.

4 IDENTIFICATION OF SUBMM-BRIGHT NIRGS

4.1 Method of identification

In order not to miss any candidate submm-bright NIRGs, we utilized two SCUBA $850\text{-}\mu\text{m}$ maps which have different pixel size produced by independent reductions and reported in Coppin et al. (2006 – Reductions B and D). The pixel sizes of the SCUBA $850\text{-}\mu\text{m}$ map from Reductions B and D are $1''$ and $3''$, respectively. One benefit of using SCUBA maps, rather than the SHADES source catalogue, is the possibility of identifying additional submm sources which are just below the limit of the SHADES catalogue. This is a reasonable approach, since we know the sky positions of targets beforehand (and see Appendix A for a statistical discussion).

We adopted the threshold of $S/N > 3$ for the detection of submm fluxes at the positions of NIRGs. In order to confirm the detection of NIRGs in SCUBA maps, we need to exclude the possibility of; 1) chance association with a nearby SCUBA source; and 2) false positive detections. Sources in the SHADES catalogue should be quite reliable, since they are extracted using 4 independent reductions. If there are no SHADES catalogue sources corresponding to detected NIRGs, we need to pay special attention to check the reliability of the detection in the SCUBA map. To overcome these problems, we use the *Spitzer* images at $24\mu\text{m}$ and the VLA radio images at 1.4 GHz as they have proved to be useful in previous studies (e.g. Ivison et al. 2002; Egami et al. 2004). The identification of SHADES sources has been undertaken by Ivison et al. (2007). We confirmed that our results are consistent with their identifications. For non-SHADES sources, we require detection at $24\mu\text{m}$ or in the radio for secure identification of submm-bright NIRGs.

We also obtained $450\text{-}\mu\text{m}$ images simultaneously with the $850\text{-}\mu\text{m}$ images, although the weather conditions allocated for SHADES were not good enough to detect typical $850\text{-}\mu\text{m}$ sources at $450\mu\text{m}$ in the same integration time. We have however used the $450\mu\text{m}$ map to constrain the $450\text{-}\mu\text{m}$ flux for the detected $850\text{-}\mu\text{m}$ sources. The reduction of $450\mu\text{m}$ data is fully described in Coppin et al. (2006).

4.2 Results

Among 307 NIRGs in the SHADES/SIRIUS K_s -band area (245 fall in J -band area), we detected 5 NIRGs at $850\mu\text{m}$ as a result of photometry at the position of NIRGs in the SHADES B-map (i.e. the SCUBA $850\mu\text{m}$ map from Reduction B). We also detected 5 NIRGs at $850\mu\text{m}$ in the SHADES D-map, four of which are common with those detected in the SHADES B-map. The results of the sub-mm detections from both SHADES maps are summarised in Table 2. All of the submm-detected NIRGs except for ID1390 have corresponding SHADES catalogue sources. Although a submm source for ID1390 (SXDF850.62) was included in a preliminary SHADES source catalogue, this source did not satisfy the final significance limit adopted for the SHADES catalogue presented by Coppin et al. (2006). However, we found that ID1390 is detected both at $24\mu\text{m}$ and in the radio, and therefore we conclude that this is a real submm galaxy (see also Appendix A). In the $450\text{-}\mu\text{m}$ map, we find no convincing detections at the positions of NIRGs. This

is not unexpected given the high noise level in the $450\mu\text{m}$ maps.

Three (ID300, 445, 912) out of six submm-detected NIRGs are identified as optical counterparts of corresponding SHADES sources in Ivison et al. (2007). Additionally, we find ID1390 as an optical-NIR counterpart of SXDF850.62 (a non-SHADES source), since this galaxy is detected at $24\mu\text{m}$ and in the radio as noted above. In summary, we identify four submm-bright NIRGs. Figure 3 shows the $850\text{-}\mu\text{m}$ contours plotted over K_s -band images of submm-bright NIRGs. Figure 3 also shows the radio contours over R -band images of the same NIRGs. The remaining two submm-detected NIRGs (ID718 and ID1133) are detected neither in the radio nor at $24\mu\text{m}$. Such chance associations are expected and the number is consistent with the estimate given in Appendix A. For a submm source associated with ID1133, Ivison et al. (2007) found another reliable optical counterpart with a radio detection. Considering these results, we exclude both ID718 and 1133 from further analyses.

In order to check additional candidates for optical-NIR counterparts of the SHADES catalogue sources, we also searched for NIR-selected galaxies within $7''$ radius of the SHADES positions. Although we found two additional associations (ID475 and 579), they are not detected either at $24\mu\text{m}$ or in the radio. Therefore, this alternative method does not produce any further submm-bright NIRGs for our sample.

4.3 Relation between submm galaxies and NIRGs

In Table 3, we tabulate the optical-NIR properties of submm-bright NIRGs. Note that all of the submm-bright NIRGs are BzK -selected galaxies, except for ID1390 with $BzK = -0.36$, although it satisfies $BzK \geq -0.2$ before the colour correction on $B - z$ and $z - K$. This also means that no EROs and DRGs which are clearly *non-BzK* galaxies are detected at $850\mu\text{m}$. The distribution of submm-bright NIRGs in the $B - z$ vs $z - K$ colour-colour diagram is discussed in detail in Section 6.1.

Two galaxies, ID300 and ID445, satisfy all the colour selection criteria we adopted, i.e. $BzK \geq -0.2$, $R - K > 3.35$ and $J - K > 1.32$. Hereafter, we refer to this BzK -DRG-ERO overlapping population as extremely red BzK -selected galaxies. We found only 16 extremely red BzK s in the combined K_s and SHADES areas, corresponding to a surface density of only $0.25 \pm 0.05 \text{ arcmin}^{-2}$. This means that $12 \pm 8\%$ $(2/16)^3$ of extremely red BzK s are submm galaxies. Although the sample is very small, nevertheless it may indicate that this rare NIR galaxy population has a much higher fraction of submm galaxies, compared with the other optical-NIR selected galaxy populations already studied. For example, the fractions of submm galaxies which are BzK s, EROs and DRGs in our sample are $4/132$ ($3 \pm 2\%$), $3/201$ ($1.5 \pm 1\%$) and $3/67$ ($5 \pm 3\%$), respectively.

We found that there are 20 (13) SHADES sources in the SIRIUS/ K_s -band (J -band) area, among which three are

BzK -selected and two satisfy both the ERO and DRG selection. The resulting fractions of BzK s, EROs and DRGs in our sub-sample of SHADES sources are $15 \pm 8\%$, $10 \pm 7\%$ and $15 \pm 10\%$, respectively. Thirteen SHADES sources out of 20 have a robust radio identification (Ivison et al. 2007). If we confine our attention to SHADES sources with a robust radio identification, the above fractions of NIRGs are higher by a factor of ~ 1.5 .

Ivison et al. (2002) found an ERO fraction of 33% ($6/18$) in SCUBA sources with robust radio identification from the 8-mJy survey, in which one ERO is too faint to be detected at our detection limit in the K_s -band. Reddy et al. (2005) studied the BzK and DRG fraction of submm galaxies with $S_{850\mu\text{m}} \gtrsim 5 \text{ mJy}$ in the GOODS-North field. Out of 11 radio-detected submm galaxies, they found that 5 ($45 \pm 15\%$) and 3 ($27 \pm 13\%$) objects satisfy the BzK and DRG criteria, respectively. For these submm-bright BzK and DRG samples, 2 objects each are too faint to be detected at our detection limits. Subtracting these K -band faint sources would give the BzK and DRG fractions of $27 \pm 13\%$ and $9 \pm 8\%$, respectively. On the other hand, Daddi et al. (2005) found only one BzK -selected galaxy in the list of submm sources in Pope et al. (2005) in the GOODS-North field. These results are not inconsistent with ours, considering the large errors, due to a small sample size and cosmic variance.

Since the redshift distribution of BzK s has a large overlap with that of submm galaxies, and both classes of object are star-forming galaxies, one could expect a large fraction of BzK s within the submm galaxy population. We roughly estimate the expected fraction of BzK s in submm galaxy samples as follows, based on the results of the redshift survey of radio-detected submm galaxies by Chapman et al. (2005). In their sample of radio-detected submm galaxies, the fraction of galaxies at $1.4 < z < 2.5$ is about 45% . This fraction should be corrected for the incompleteness of the sample, mainly due to the redshift desert at $1.2 < z < 1.8$. Given the 20% incompleteness at $z \simeq 1.2\text{--}1.8$ estimated by Chapman et al. (2005), the fraction of galaxies at $1.4 < z < 2.5$ may be in the range of $35\text{--}45\%$. If BzK s are an almost complete sample of star-forming galaxies at $1.4 < z < 2.5$, including heavily obscured objects, most of radio-detected submm galaxies at $1.4 < z < 2.5$ may be selected as BzK s. In our SHADES/SIRIUS field, there are 13 radio-detected SHADES catalogue sources. Therefore, one may expect that 4–6 of them are BzK s. From the K -band magnitude of radio-detected submm galaxies of Smail et al. (2004), we found that $\sim 65\%$ of radio-detected submm galaxies are detectable at the detection limit of our K_s -band image. Thus, we expect that at most ~ 4 radio-detected submm galaxies would be BzK s in our sample. This rough estimate is consistent with the results above, since we found 3 such radio-detected submm galaxies. Although the sample is small, this suggests that the BzK selection technique is effective even for submm galaxies, i.e. heavily obscured galaxies with extremely high SFR. Thus, submm galaxies at $z \sim 2$ may have the largest overlap with BzK -selected galaxies, when compared to EROs and DRGs. In Section 6.2.3, we discuss the implications of this, using a radiative transfer model of starburst galaxies.

The results presented here are hampered by small sample size, partly due to the limited overlap between our NIR

³ The errors on fractions, f , are given by $\sqrt{\frac{f(1-f)}{n}}$ where n is the total number of the sample. This gives a rough estimate based on the normal approximation to the binomial distribution.

images and the SHADES field. Both of the SHADES fields have been covered by the UKIRT Infrared Deep Sky Survey (UKIDSS – Lawrence et al. 2006). In the near future it will therefore be possible to study the submm properties of a large sample of NIRGs using the UKIDSS data.

5 STACKING ANALYSIS FOR SUBMM-FAINT NIRGS

We can try to extract a little more information about the submm galaxies/NIRG overlap by looking at the statistical correlations within the images. Here we estimate the average 850- μm flux of submm-faint NIRGs and the contribution to the extragalactic background light (EBL) from each class of objects.

We first eliminated the effects of resolved submm sources in our SCUBA maps. In the B-map, we excluded regions within $7''$ of the SHADES catalogue sources. In the D-map, all the SHADES sources and their associated negative off-beams were removed before measuring the flux. For this cleaned D-map, we confirmed that random positions give a variance-weighted average flux of zero. Although a non-SHADES source for ID1390 is not removed from the maps, its effect is negligible.

In Figures 4–6, we show the histogram of measured flux at the position of NIRGs in the B-map, compared with that of the map as a whole. The significance of the difference between the distributions of the map and the measured fluxes was estimated with the Kolmogorov-Smirnov test. The flux distributions of *BzKs* and EROs were found to be different from that of the map as a whole, with a significance of $2\text{--}3\sigma$ (see Table 4). For DRGs, we found no significant detection from the Kolmogorov-Smirnov test using 56 objects. As a comparison, Knudsen et al. (2005) detected an average flux of 0.74 ± 0.24 mJy for DRGs (excluding discrete sources) with a smaller sample of 30, but with a lower noise SCUBA map. A possibly large contamination in our DRG sample, owing to the shallow *J*-band data, might cause no significant detection.

From the B-map, we obtained an average flux of 0.52 ± 0.19 and 0.53 ± 0.16 mJy for *BzKs* and EROs, respectively. We measured the average flux of data between the first and the third quartiles of the sample, which is a robust measure against outliers. The errors are given by the median absolute deviation. Table 4 gives a summary of the stacking analysis using the B-map. The noise-weighted average flux of *BzKs*, EROs, and DRGs measured in the D-map is 0.64 ± 0.16 , 0.50 ± 0.13 and 0.42 ± 0.23 mJy, respectively, which are consistent with the results from the B-map. The derived average fluxes of *BzKs* and EROs are consistent with previous studies in other sky regions (Webb et al. 2004; Daddi et al. 2005)⁴. In the following discussion, we use the average flux of submm-faint *BzKs* and EROs from the B-map.

We next estimate the contribution from each class of object to the EBL at 850 μm . The total flux from individually detected sources is added to the estimated total flux

from undetected objects. The values obtained for the EBL from *BzKs* and EROs are 3.8 ± 1.2 and 5.1 ± 1.5 Jy deg^{-2} , respectively. The measured 850 μm EBL is 31 Jy deg^{-2} in Puget et al. (1996) and 44 Jy deg^{-2} in Fixsen et al. (1998), i.e. there is a relatively large uncertainty on the absolute level. The contribution from *BzKs* and EROs are both 10–15 % each, depending on the adopted value of the EBL. This modest contribution is also suggested by a comparison of the surface density of objects. For example, the surface density of *BzKs*, ~ 1.5 arcmin^{-2} is a factor of ~ 5 smaller than that of >0.5 mJy SCUBA sources, ~ 7 arcmin^{-2} (Blain et al. 1999; Cowie et al. 2002) at which flux density level the background is close to complete.

We also estimate the resolved fraction of the EBL originating from a given galaxy population only. The resolved fraction of the EBL from *BzKs* is at least $\sim 30\%$, which could be higher than that found in EROs. The detected sources in our sample correspond to $\gtrsim 3.5\sigma$ sources when we measure the peak flux in the SCUBA map with the noise level of ~ 2 mJy. From the 8-mJy survey, which has a similar noise level, Scott et al. (2002) found that $\gtrsim 3.5\sigma$ sources account for $\simeq 10\%$ of the EBL. Thus, the submm flux of *BzKs* is apparently biased high; i.e. a large fraction of the submm fluxes from *BzKs* are found in resolved bright sources.

Recently, Wang et al. (2006) suggested that the majority of the EBL at 850 μm originates from submm-undetected galaxies at $z \lesssim 1.5$. On the other hand, the majority of submm-detected galaxies, i.e. resolved sources, lie at $z \gtrsim 1.5$ (Chapman et al. 2005). This suggests that the resolved fraction of the EBL varies as a function of redshift. If we study the EBL only from galaxy populations at $z \gtrsim 1.5$ like *BzKs*, the contribution from submm-undetected galaxies to the EBL would be significantly reduced. This may explain why the resolved fraction of the EBL from $z \sim 2$ *BzKs* is higher than that from EROs typically at $z \sim 1$.

6 SED ANALYSIS OF SUBMM-BRIGHT NIRGS

In this section, we investigate the physical properties of submm-bright NIRGs from the observed SEDs. Firstly, we examine the distribution of submm-bright NIRGs in the *B* – *z* vs *z* – *K* colour-colour plot, i.e. *BzK* diagram. Specifically, we compare the properties of submm-bright NIRGs with those of 24 μm -detected NIRGs. Secondly, we apply an evolutionary SED model of starbursts to submm-bright NIRGs for a more detailed study of each object. Also, we study the properties of submm-faint NIRGs from an average SED, which are compared with those of submm-bright NIRGs.

6.1 Submm-bright NIRGs in the *BzK* diagram

The fraction of *BzKs* in a galaxy population would depend on its redshift distribution; i.e. low-*z* galaxy population would have a small fraction of *BzKs*. Figure 7 shows the *BzK* diagram for all the *K_s*-detected objects in the SXDF/SIRIUS field. While NIRGs have a wide range of *B* – *z*, i.e. $0 \lesssim (B - z) \lesssim 6$, submm-bright NIRGs favour the colour range $1 \lesssim (B - z) \lesssim 3$, with *BzK* $\gtrsim -0.2$. This is not the case for general 24 μm -detected objects, which have

⁴ Note that Daddi et al. (2005) derived an average flux of 1.0 ± 0.2 mJy for ‘24 μm -detected’ *BzKs*. Including 24 μm -undetected objects, this average becomes 0.63 ± 0.17 mJy in the GOODS-North field

$0.5 \lesssim (B - z) \lesssim 4$ and a large fraction of non-*BzKs*. Unlike $24\ \mu\text{m}$ -detected NIRGs, submm-bright NIRGs disfavour non-*BzK* EROs and are better matched to the $B - z$ colours of *BzKs*. This is consistent with the redshift distribution of radio-detected submm galaxies, having a median of $z \sim 2$ (Chapman et al. 2005), which overlaps considerably with that of *BzKs*. On the other hand, $24\ \mu\text{m}$ -detected objects include a large number of $z \lesssim 1.5$ galaxies (Rowan-Robinson et al. 2005), and have a small *BzK* fraction.

Note that $24\ \mu\text{m}$ -detected NIRGs include fairly blue *BzKs* with $(B - z) \lesssim 1$, unlike submm-bright ones. The correlation between $B - z$ and reddening for *BzK*-selected galaxies is discussed by Daddi et al. (2004), suggesting that $E(B - V) = 0.25(B - z + 0.1)$ for the Calzetti extinction law (Calzetti et al. 2000). According to this relation, $(B - z) \lesssim 1$ corresponds to $E(B - V) \lesssim 0.3$. On the other hand, we derive $E(B - V) \simeq 0.5$ for submm-bright *BzKs* on average from $\langle B - z \rangle = 2.1$. Reddy et al. (2005) show that UV-selected ‘BX/BM’ galaxies occupy a region in the *BzK* diagram similar to *BzK*-selected galaxies with $(B - z) \lesssim 1$. Since these UV-selected galaxies are less obscured by dust than submm galaxies (e.g. Smail et al. 2004), it is expected that most submm-bright NIRGs may avoid the colour region of $(B - z) \lesssim 1$.

The other possibilities for blue $B - z$ colours include the presence of AGN. We performed a cross-correlation between the $24\ \mu\text{m}$ -detected *BzK* sample and X-ray sources in the XMM serendipitous source catalogue⁵. As a result, we found that the bluest four $24\ \mu\text{m}$ -detected *BzKs* with $(B - z) \lesssim 1$ and $(z - K) \lesssim 1$ are associated with X-ray sources with an angular distance of $\theta < 2''$, while the submm-bright sample have no such associations. Therefore, bluer colours of $24\ \mu\text{m}$ -detected *BzKs* appear to be better explained by a contribution from AGN.

In summary, the colours of submm-bright NIRGs, $1 \lesssim (B - z) \lesssim 3$, indicate that they are obscured star-forming galaxies at $z \gtrsim 1.4$, with no obvious contribution from AGN to the observed optical-NIR fluxes. The nature of submm-bright NIRGs is further discussed below using multi-wavelength data and a theoretical SED model.

6.2 Comparison with SED models

6.2.1 SED fitting method

We analyse the SEDs of submm-bright NIRGs using an evolutionary SED model of starbursts of Takagi et al. (2003) which has previously been applied to submm galaxies in Takagi et al. (2004). In this model, the equations of radiative transfer are solved for a spherical geometry with centrally concentrated stars and homogeneously distributed dust. We use the same model templates as those used in Takagi et al. (2004). We hereafter refer to this model as the StarBURst Radiative Transfer (SBURT) model. Here we extend the wavelength range of the SBURT model to the radio by assuming the observed correlation between far-IR and radio emission (Condon 1992), with $\alpha = -0.75$ and $q = 2.35$,

where α is the spectral index of radio emission ($S_\nu \propto \nu^\alpha$) and q defines the luminosity ratio of far-IR to radio emission at 1.49 GHz (see Condon 1992).

The fitting parameters of the SBURT model are the redshift, starburst age and compactness of a starburst region (Θ). The evolutionary time-scale of the starbursts t_0 is assumed to be 0.1 Gyr, which specifies both the gas infall rate and the star formation rate. The compactness of starbursts is defined by $r = \Theta(M_*/10^9 M_\odot)^{\frac{1}{2}}$ [kpc], where r and M_* are the radius and stellar mass of the starburst region, respectively. The dust model is chosen from the MW, LMC or SMC models taken from Takagi et al. (2003). Following the results of Takagi et al. (2004), we adopt a top-heavy initial mass function (IMF) with a power law index of $x = 1.10$ (the Salpeter IMF has $x = 1.35$) for submm galaxies, which is necessary to reproduce the colour-magnitude relation of present-day elliptical galaxies. The lower and upper mass limits of the adopted IMF are 0.1 and $60 M_\odot$, respectively. This particular choice of the IMF does not affect the following results, except for the derived stellar masses.

The best-fitting SED model is searched for using a χ^2 -minimization technique from the prepared set of SED models. We used all the available fluxes, except for $24\ \mu\text{m}$ and radio. This is because, in the SBURT model; 1) the contribution from an AGN is not taken into account; 2) the $24\ \mu\text{m}$ flux depends on the details of the dust model; and 3) the radio flux is separately calculated by using the empirical relation. The adopted 850- μm fluxes and errors are ‘deboosted values’ (i.e. accounting for the effects of flux boosting on a low S/N threshold sample) taken from Coppin et al. (2006) or calculated with the same deboosting algorithm. We adopted a minimum flux error of 5%, considering the systematic uncertainty of photometry from the different type of instruments covering a wide range of wavelength. The upper limits on fluxes are taken into account in the fitting process, i.e. models exceeding the 5σ upper limits are rejected. At rest frame UV wavelengths, the SEDs of heavily obscured starbursts like submm galaxies could depend on the inhomogeneity of interstellar medium, since the effects of photon leakage may dominate the resulting SED (e.g. Takagi et al. 2003). Also, the absorption by the intergalactic medium is important in the rest frame below 1216 Å, which depends on a particular line of sight to each galaxy. Considering these uncertainties, we quadratically added an additional 20% error for data at rest-frame UV wavelengths below 4000 Å.

6.2.2 Results of SED fitting

In Figure 8, we show the best-fitting models for submm-bright NIRGs. The original and radio-extended SBURT models are depicted with solid and dotted lines, respectively. The fitting and derived model parameters are summarised in Table 5.

For ID912, we found that the value of minimum χ^2 reduced drastically when we excluded *H*-band data from the fitting analysis. This may indicate that the *H*-band photometry could have a large systematic error. The upper limit in the *J*-band suggests that this galaxy could be very red in the observed NIR colours. The noise level in the *H*-band may be too high to detect this galaxy. We checked the images of

⁵ The XMM-Newton Serendipitous Source Catalogue, version 1.1.0, XMM-Newton Survey Science Centre Consortium, XMM-SSC, Leicester, UK (2004)

ID912 and found that photometry of this galaxy could be affected by a nearby object. Hence, we adopt the best fitting model for ID912 without H -band data.

We find a significant underestimate of $850\ \mu\text{m}$ flux for ID445 which has a very red $z' - K_s$ colour, although the resulting χ^2 value indicates that the best-fitting model is statistically acceptable. Since the predicted radio flux is also well below the observed flux, the best-fitting model might be rejected with more accurate measurements in the submm. For this source, we may particularly need a more complicated multi-component model of starbursts, in which young heavily obscured molecular clouds are treated separately (e.g. Silva et al. 1998).

The SED fitting suggests that submm-bright NIRGs could lie at the typical redshift range of submm galaxies (Chapman et al. 2005). In order to show the fitting error on photometric redshifts z_{phot} , we show contour plots of $\Delta\chi^2$ projected onto the age-redshift plane in Figure 9 for models with the best dust model for each galaxy. We note that the derived z_{phot} and the far-IR-radio relation reproduce the observed radio flux well, except for ID445.

At $24\ \mu\text{m}$, we find that the observed fluxes are typically higher than the model predictions, while the model flux of ID912 is consistent with the observed $24\ \mu\text{m}$ flux. We regard the model flux at $24\ \mu\text{m}$ as the lower limit for the following reasons: 1) lack of AGN contribution in the model; and 2) the non-MW dust models are preferentially selected from the featureless SED at rest-frame UV, which may have a lower MIR emissivity than actual dust grains in submm galaxies. Specifically, the lack of AGN could be important for submm galaxies, in which the AGN activity to some extent is already known (Alexander et al. 2005). Recently, Daddi et al. (2007) found a galaxy population at $z \sim 2$ which shows a distinct excess of flux at $24\ \mu\text{m}$, compared to that expected from the SFR estimated at other wavelengths. This MIR excess is attributed to Compton-thick AGNs, as a result of stacking analysis of deep X-ray images. Submm-bright NIRGs showing a clear excess of flux at $24\ \mu\text{m}$ (ID300 and 1390), might be such MIR-excess galaxies.

Submm-bright NIRGs are found to be massive, with the stellar masses of 5×10^{10} – $10^{11}\ M_{\odot}$. The derived bolometric luminosity of 3×10^{12} – $10^{13}\ L_{\odot}$ (excluding ID445) corresponds to the star formation rate of ~ 300 – $1000\ M_{\odot}\ \text{yr}^{-1}$ for the adopted top-heavy IMF. For the Salpeter IMF, the stellar mass and the SFR could be even a few times higher than we derived.

Following Takagi et al. (2004), we predict the present-day colours and absolute magnitudes of submm-bright NIRGs. Since we assume that the effects of star formation after the observed epoch is negligible, the derived present-day colours and luminosities are both lower limits. These lower limits could be close to reasonable values for ID300 and 1390, which seem to be well evolved starbursts with $t/t_0 \gtrsim 2$ and $M_{\text{star}} > M_{\text{gas}}$. For these galaxies, we predict absolute V -band magnitudes of $M_V = -20.7$ to -20.1 , while submm-faint BzK s would have $M_V = -19.4$ on average. Since we use a top-heavy IMF, this magnitude is ~ 1 mag fainter than those by the Salpeter IMF. We find that the predicted rest-frame $U - V$ and M_V are consistent with the colour-magnitude relation of elliptical galaxies. This is not the case for the Salpeter IMF (see also Takagi et al. 2004).

6.2.3 Colour evolution of the SBURT model

In Section 4, we mentioned the possibility that submm galaxies have a much larger overlap with BzK -selected galaxies, compared with EROs and DRGs. In Figure 10, we show the BzK , $R - K$, and $J - K$ colours as a function of starburst age at $z = 2$, i.e. a typical redshift for submm galaxies. We choose $\Theta = 0.7$ – 1.4 , which results in a good match with the observed SED variation of submm galaxies for the SMC dust model (see Takagi & Pearson 2005). The SBURT models satisfy $BzK \gtrsim -0.2$ for a wide range of model parameters, i.e. starburst age and compactness of the starburst region (or optical depth). On the other hand, $R - K > 3.35$ is only satisfied with old models having $t/t_0 \gtrsim 3$ for a wide range of Θ . This is also true for DRGs, except for a small fraction of models. Therefore, in the SBURT model, SEDs of stellar populations need to be intrinsically red to reproduce the colours of EROs and DRGs. Thus, this model predicts the largest overlap between BzK s and submm galaxies, among NIRGs. If we assume the limit on starburst age of $t/t_0 \sim 6$ (Takagi et al. 2004), we expect the number of BzK s in submm galaxies to be about twice that of EROs, given that the selection of BzK s and EROs are not sensitive to the compactness Θ . This prediction could be confirmed by using larger samples of submm-bright NIRGs.

6.2.4 Why are some BzK s bright in submm?

In this study, we found that only a handful of NIRGs are bright in the submm. So, are submm-bright ones experiencing a special luminous evolutionary phase or simply more massive than submm-faint ones? If the former is the case, the duty cycle of submm-bright BzK s may be estimated from the fraction of submm-bright NIRGs. In the following discussion, we focus only on BzK s, since EROs and DRGs could be contaminated by passively evolving galaxies. We found that only 3% of BzK s are bright in submm. This indicates that the duty cycle of submm-bright BzK s is only $< 10\%$ of the star-forming phase, even if we consider the incompleteness of the SHADES survey (Coppin et al. 2006). Thus, we might be observing a very sharp peak in the star formation activity of BzK s (e.g. see also Dannerbauer et al. 2006). If this is the case, the SEDs of submm-bright BzK s may be systematically different from those of submm-faint ones.

In order to address this question, we derived the average SED of submm-faint BzK s with $1.5 < (B - z) < 2.5$, i.e. having similar colour to submm-bright ones. In Figure 11, we show the average SED of 65 submm-faint BzK s with $1.5 < (B - z) < 2.5$. At $850\ \mu\text{m}$, we adopted the average flux of BzK s derived from our stacking analysis. The average flux of submm-faint BzK s in the radio were also derived with a stacking analysis, and found to be $f_{1.4\text{GHz}} = 5.7 \pm 1.0\ \mu\text{Jy}$. A representative model⁶ for the average SED was sought with the same method used for individual submm-bright galaxies. For the flux error at optical-NIR bands, we adopted the standard deviation of the sample at each photometric band. Since this error is rather large, we fixed the redshift to the

⁶ We call this model not the ‘best’ but ‘representative’, since the variance of the average SED is too large to specify one particular model as the best one.

average redshift of $BzKs$, $\langle z \rangle = 1.9$ (Daddi et al. 2004), in order to constrain the parameter space. We show the model thus obtained in Figure 11. The model parameters are tabulated in Table 5.

Although the uncertainty is large, the average SED thus derived is not very much different from those of submm-bright $BzKs$, and reasonably explained by the the SBURT model, i.e. a starburst model, not mild evolutionary models for quiescent galaxies. Therefore, from the SED analysis, we found no clear signatures that the evolutionary phase of submm-bright $BzKs$ is substantially different from that of submm-faint ones. Compared to submm-bright galaxies, a difference in the model parameters may be found in the mass scale, i.e. submm-faint ones are less massive. Since the representative model is an old model of a starburst, the estimated mass is close to the upper limit, owing to a higher mass-to-light ratio compared with younger models. From an oldest model which reproduces the average SED, we derive the upper limit on the stellar mass as $M_{\text{star}} \lesssim 5 \times 10^{10} M_{\odot}$. Compared to the oldest submm-bright NIRG in our sample, ID1390 (excluding ID445), the stellar mass of submm-faint $BzKs$ could be less than half of ID1390. This may suggest that submm-bright and faint $BzKs$ evolve into galaxies with different stellar masses, rather than being galaxies of a similar stellar mass but in different evolutionary stages. We however caution that the sample size of submm-bright $BzKs$ are too small to derive firm conclusions on their average physical properties, such as stellar mass. We need a larger sample of submm-bright $BzKs$, and spectroscopic redshifts for more secure analyses. Also note that the mass estimate of the SBURT model may suffer from systematic effects, owing to the assumed simple star/dust geometry.

7 SUMMARY

We have investigated the submm properties of the following classes of NIR-selected galaxies: BzK -selected star-forming galaxies; DRGs; and EROs. We utilised a 93 arcmin^2 sub-region of the SHADES SXDF $850 \mu\text{m}$ map which has already been imaged in the NIR with the SIRIUS camera on the UH 2.2m telescope.

Using two SCUBA $850\text{-}\mu\text{m}$ maps (the SHADES B-map and D-map) produced by two different groups within the SHADES consortium, we detected 6 NIRGs above 3σ . Four submm-detected NIRGs out of six are also detected both at $24 \mu\text{m}$ and in the radio. This suggests that these 4 submm-detected NIRGs are genuine submm-bright galaxies. These submm-bright NIRGs are all BzK -selected galaxies, except for ID1390 whose BzK colour is however close to the selection boundary. In other words, no EROs and DRGs are found to be submm-bright if they are clearly non- $BzKs$. We made a rough estimate of the number of $BzKs$ in radio-detected submm galaxies, assuming that submm galaxies at $1.4 < z < 2.5$ satisfy the selection criteria of $BzKs$. Although the sample is small, this estimate is consistent with our result. This may indicate that most submm galaxies at $1.4 < z < 2.5$ could be $BzKs$.

Two submm-detected NIRGs satisfy all the selection criteria we adopted, i.e. they are extremely red BzK -selected galaxies. Although these extremely red $BzKs$ are rare, the fraction of submm galaxies in them could be

high (up to 20%), compared with the other colour-selected optical-NIR galaxy populations.

We performed stacking analyses with our SCUBA $850\text{-}\mu\text{m}$ maps, in order to derive the average flux of submm-faint NIRGs. We derived 0.52 ± 0.19 (0.64 ± 0.16) mJy and 0.53 ± 0.16 (0.50 ± 0.13) mJy from the B-map (D-map) for $BzKs$ and EROs, respectively, while we found no significant signal from DRGs in either map. The contribution from $BzKs$ and EROs to the EBL at $850 \mu\text{m}$ is about 10–15%. Focusing on the EBL only from $BzKs$, we found that $\gtrsim 30\%$ of the EBL from $BzKs$ is resolved in our SCUBA map. This is higher than that for EROs and submm sources as a whole. This might be expected if the majority of the EBL originates from submm-undetected galaxies at $z < 1.5$, as suggested by Wang et al. (2006). For galaxies at $z \sim 2$, the fraction of submm flux in resolved sources could be higher than that in low- z galaxies.

We have also fitted SED models of starbursts to each of the submm-bright NIRG (mostly $BzKs$) and to an average SED of submm-faint $BzKs$ derived from galaxies with $1.5 < (B - z) < 2.5$, i.e. similar colours to the submm-bright ones. Submm-bright NIRGs are found to lie at the typical redshifts of submm galaxies and have stellar masses of $5 \times 10^{10} - 10^{11} M_{\odot}$ with a Salpeter-like, but slightly top-heavy IMF and bolometric luminosity of $3 \times 10^{12} - 10^{13} L_{\odot}$. From the average SED of submm-faint $BzKs$, we found no clear signature that the evolutionary phase of submm-bright $BzKs$ are substantially different from that of submm-faint ones, as suggested by the small number of submm-bright $BzKs$. On the other hand, submm-faint $BzKs$ are likely to be less massive, with the stellar mass below $\sim 5 \times 10^{10} M_{\odot}$.

The results presented here are clearly limited by small sample size. Nevertheless, our study can still be considered useful for investigating the physical relationships between NIR-selected and submm-selected massive galaxies. A large sample of submm-bright NIRGs from currently ongoing and future multi-wavelength surveys, including SHADES and UKIDSS will play an important role on the study of massive galaxy formation and evolution.

ACKNOWLEDGMENTS

We thank all the members of the SHADES consortium, and acknowledge continuous support from the staff of the JCMT. We also thank all the members of the SIRIUS team and acknowledge the SWIRE project team. We thank E. Daddi for useful discussions on the BzK -selection technique. TT acknowledges the Japan Society for the Promotion of Science (JSPS – PD fellow, No. 18-7747). TT and SS acknowledge support by the Particle Physics and Astronomy Research Council under grant number PPA/G/S/2001/00120/2. IRS acknowledges support from the Royal Society. This work is partly supported by a Grant-in-Aid for Scientific Research (No. 14540220) by the Japanese Ministry of Education, Culture, Sports, Science and Technology. KC and AP acknowledge the National Science and Engineering Research Council of Canada (NSERC). IA and DHH acknowledge partial support from Conacyt grants 39548-F and 39953-F. The JCMT is operated by the Joint Astronomy Centre on behalf of the UK Particle Physics and Astronomy Research Council, the

Canadian National Research Council and the Netherlands Organization for Scientific Research.

REFERENCES

- Alexander D. M., Bauer F. E., Chapman S. C., Smail I., Blain A. W., Brandt W. N., Ivison R. J., 2005, *ApJ*, 632, 736
- Arnouts S., Walcher C. J., Le Fevre O., Zamorani G., Ilbert O., Pozzetti L., Bardelli S., Tresse L., Zucca E., Le Brun V., et al. 2007, *ArXiv e-prints*, 705
- Bertin E., Arnouts S., 1996, *A&AS*, 117, 393
- Blain A. W., Chapman S. C., Smail I., Ivison R., 2004, *ApJ*, 611, 725
- Blain A. W., Kneib J.-P., Ivison R. J., Smail I., 1999, *ApJ*, 512, L87
- Borys C., Chapman S., Halpern M., Scott D., 2003, *MNRAS*, 344, 385
- Borys C., Scott D., Chapman S., Halpern M., Nandra K., Pope A., 2004, *MNRAS*, 355, 485
- Calzetti D., Armus L., Bohlin R. C., Kinney A. L., Koornneef J., Storchi-Bergmann T., 2000, *ApJ*, 533, 682
- Caputi K. I., Dole H., Lagache G., McLure R. J., Puget J.-L., Rieke G. H., Dunlop J. S., Le Floch E., Papovich C., Pérez-González P. G., 2006, *ApJ*, 637, 727
- Chapman S. C., Blain A. W., Smail I., Ivison R. J., 2005, *ApJ*, 622, 772
- Cimatti A., Daddi E., Mignoli M., Pozzetti L., Renzini A., Zamorani G., Broadhurst T., Fontana A., Saracco P., Poli F., Cristiani S., D’Odorico S., Giallongo E., Gilmozzi R., Menci N., 2002, *A&A*, 381, L68
- Cimatti A., Daddi E., Renzini A., Cassata P., Vanzella E., Pozzetti L., Cristiani S., Fontana A., Rodighiero G., Mignoli M., Zamorani G., 2004, *Nature*, 430, 184
- Condon J. J., 1992, *ARA&A*, 30, 575
- Coppin K., Chapin E. L., Mortier A. M. J., Scott S. E., Borys C., Dunlop J. S., Halpern M., Hughes D. H., Pope A., Scott D., Serjeant S., Wagg J., Alexander D. M., et al. 2006, *MNRAS*, 372, 1621
- Coppin K., Halpern M., Scott D., Borys C., Chapman S., 2005, *MNRAS*, 357, 1022
- Cowie L. L., Barger A. J., Kneib J.-P., 2002, *AJ*, 123, 2197
- Daddi E., Alexander D. M., Dickinson M., Gilli R., Renzini A., Elbaz D., Cimatti A., Chary R., Frayer D., Bauer F. E., Brandt W. N., Giavalisco M., Grogin N. A., Huynh M., Kurk J., Mignoli M., Morrison G., Pope A., Ravindranath S., 2007, *ArXiv e-prints*, 705
- Daddi E., Cimatti A., Pozzetti L., Hoekstra H., Röttgering H. J. A., Renzini A., Zamorani G., Mannucci F., 2000, *A&A*, 361, 535
- Daddi E., Cimatti A., Renzini A., Fontana A., Mignoli M., Pozzetti L., Tozzi P., Zamorani G., 2004, *ApJ*, 617, 746
- Daddi E., Cimatti A., Renzini A., Vernet J., Conselice C., Pozzetti L., Mignoli M., Tozzi P., Broadhurst T., di Serego Alighieri S., Fontana A., Nonino M., Rosati P., Zamorani G., 2004, *ApJ*, 600, L127
- Daddi E., Dickinson M., Chary R., Pope A., Morrison G., Alexander D. M., Bauer F. E., Brandt W. N., Giavalisco M., Ferguson H., Lee K.-S., Lehmer B. D., Papovich C., Renzini A., 2005, *ApJ*, 631, L13
- Daddi E., Dickinson M., Morrison G., Chary R., Cimatti A., Elbaz D., Frayer D., Renzini A., Pope A., Alexander D. M., Bauer F. E., Giavalisco M., Huynh M., Kurk J., Mignoli M., 2007, *ArXiv e-prints*, 705
- Dannerbauer H., Daddi E., Onodera M., Kong X., Röttgering H., Arimoto N., Brusa M., Cimatti A., Kurk J., Lehnert M. D., Mignoli M., Renzini A., 2006, *ApJ*, 637, L5
- Dickinson M., Papovich C., Ferguson H. C., Budavári T., 2003, *ApJ*, 587, 25
- Drory N., Salvato M., Gabasch A., Bender R., Hopp U., Feulner G., Pannella M., 2005, *ApJ*, 619, L131
- Eales S., Lilly S., Gear W., Dunne L., Bond J. R., Hammer F., Le Fevre O., Crampton D., 1999, *ApJ*, 515, 518
- Egami E., Dole H., Huang J.-S., Pérez-Gonzalez P., Le Floch E., Papovich C., Barmby P., Ivison R. J., Serjeant S., Mortier A., et al. 2004, *ApJS*, 154, 130
- Fixsen D. J., Dwek E., Mather J. C., Bennett C. L., Shafer R. A., 1998, *ApJ*, 508, 123
- Fontana A., Donnarumma I., Vanzella E., Giallongo E., Menci N., Nonino M., Saracco P., Cristiani S., D’Odorico S., Poli F., 2003, *ApJ*, 594, L9
- Fontana A., Pozzetti L., Donnarumma I., Renzini A., Cimatti A., Zamorani G., Menci N., Daddi E., Giallongo E., Mignoli M., Perna C., Salimbeni S., Saracco P., Broadhurst T., Cristiani S., D’Odorico S., Gilmozzi R., 2004, *A&A*, 424, 23
- Franx M., Labbé I., Rudnick G., van Dokkum P. G., Daddi E., Förster Schreiber N. M., Moorwood A., Rix H., Röttgering H., van de Wel A., van der Werf P., van Starckenburg L., 2003, *ApJ*, 587, L79
- Glazebrook K., Abraham R. G., McCarthy P. J., Savaglio S., Chen H.-W., Crampton D., Murowinski R., Jørgensen I., Roth K., Hook I., Marzke R. O., Carlberg R. G., 2004, *Nature*, 430, 181
- Grazian A., Fontana A., Moscardini L., Salimbeni S., Menci N., Giallongo E., de Santis C., Gallozzi S., Nonino M., Cristiani S., Vanzella E., 2006, *A&A*, 453, 507
- Greve T. R., Bertoldi F., Smail I., Neri R., Chapman S. C., Blain A. W., Ivison R. J., Genzel R., Omont A., Cox P., Tacconi L., Kneib J.-P., 2005, *MNRAS*, 359, 1165
- Hughes D. H., Serjeant S., Dunlop J., Rowan-Robinson M., Blain A., Mann R. G., Ivison R., Peacock J., Efstathiou A., Gear W., Oliver S., Lawrence A., Longair M., Goldschmidt P., Jenness T., 1998, *Nature*, 394, 241
- Ivison R. J., Greve T. R., Dunlop J. S., et al. 2007, *ArXiv Astrophysics e-prints*
- Ivison R. J., Greve T. R., Smail I., Dunlop J. S., Roche N. D., Scott S. E., Page M. J., Stevens J. A., Almaini O., Blain A. W., et al. 2002, *MNRAS*, 337, 1
- Juneau S., Glazebrook K., Crampton D., McCarthy P. J., Savaglio S., Abraham R., Carlberg R. G., Chen H.-W., Le Borgne D., Marzke R. O., Roth K., Jørgensen I., Hook I., Murowinski R., 2005, *ApJ*, 619, L135
- Knudsen K. K., van der Werf P., Franx M., Förster Schreiber N. M., van Dokkum P. G., Illingworth G. D., Labbé I., Moorwood A., Rix H.-W., Rudnick G., 2005, *ApJ*, 632, L9
- Kong X., Daddi E., Arimoto N., Renzini A., Broadhurst T., Cimatti A., Ikuta C., Ohta K., da Costa L., Olsen L. F., Onodera M., Tamura N., 2006, *ApJ*, 638, 72
- Kovács A., Chapman S. C., Dowell C. D., Blain A. W.,

- Ivison R. J., Smail I., Phillips T. G., 2006, ApJ, 650, 592
- Labbé I., Huang J., Franx M., Rudnick G., Barmby P., Daddi E., van Dokkum P. G., Fazio G. G., Schreiber N. M. F., Moorwood A. F. M., Rix H.-W., Röttgering H., Trujillo I., van der Werf P., 2005, ApJ, 624, L81
- Lawrence A., Warren S. J., Almaini O., et al. 2006, ArXiv Astrophysics e-prints, astro-ph/0604426
- Lonsdale C. J., Smith H. E., Rowan-Robinson M., Surace J., Shupe D., Xu C., Oliver S., Padgett D., Fang F., Conrow T., Franceschini A., Gautier N., et al. 2003, PASP, 115, 897
- Miyazaki M., Shimasaku K., Kodama T., Okamura S., Furusawa H., Ouchi M., Nakata F., Doi M., Hamabe M., Kimura M., Komiyama Y., Miyazaki S., Nagashima C., et al. 2003, PASJ, 55, 1079
- Miyazaki S., Komiyama Y., Sekiguchi M., Okamura S., Doi M., Furusawa H., Hamabe M., Imi K., Kimura M., Nakata F., Okada N., Ouchi M., Shimasaku K., Yagi M., Yasuda N., 2002, PASJ, 54, 833
- Mortier A. M. J., Serjeant S., Dunlop J. S., Scott S. E., Ade P., Alexander D., Almaini O., Aretxaga I., Baugh C., Benson A. J., Best P. N., Blain A., Bock J., Borys C., et al. 2005, MNRAS, 363, 563
- Nagayama T., Nagashima C., Nakajima Y., Nagata T., Sato S., Nakaya H., Yamamuro T., Sugitani K., Tamura M., 2003, in Instrument Design and Performance for Optical/Infrared Ground-based Telescopes. Edited by Iye, Masanori; Moorwood, Alan F. M. Proceedings of the SPIE, Volume 4841, pp. 459-464 (2003). SIRUS: a near infrared simultaneous three-band camera. pp 459-464
- Papovich C., Moustakas L. A., Dickinson M., Le Floc'h E., Rieke G. H., Daddi E., Alexander D. M., Bauer F., Brandt W. N., Dahlen T., Egami E., Eisenhardt P., Elbaz D., et al. 2006, ApJ, 640, 92
- Pérez-González P. G., Rieke G. H., Egami E., Alonso-Herrero A., Dole H., Papovich C., Blaylock M., Jones J., Rieke M., Rigby J., Barmby P., Fazio G. G., Huang J., Martin C., 2005, ApJ, 630, 82
- Pope A., Borys C., Scott D., Conselice C., Dickinson M., Mobasher B., 2005, MNRAS, 358, 149
- Pope A., Scott D., Dickinson M., Chary R.-R., Morrison G., Borys C., Sajina A., Alexander D. M., Daddi E., Frayer D., MacDonald E., Stern D., 2006, MNRAS, 370, 1185
- Pozzetti L., Bolzonella M., Lamareille F., Zamorani G., Franzetti P., Le Fèvre O., Iovino A., Tempurin S., Ilbert O., Arnouts S., Charlot S., Brinchmann J., et al. 2007, ArXiv e-prints, 704
- Puget J.-L., Abergel A., Bernard J.-P., Boulanger F., Burton W. B., Desert F.-X., Hartmann D., 1996, A&A, 308, L5
- Reddy N. A., Erb D. K., Steidel C. C., Shapley A. E., Adelberger K. L., Pettini M., 2005, ApJ, 633, 748
- Rowan-Robinson M., Babbedge T., Surace J., Shupe D., Fang F., Lonsdale C., Smith G., Polletta M., Siana B., Gonzalez-Solares E., Xu K., Owen F., et al. 2005, AJ, 129, 1183
- Scott S. E., Fox M. J., Dunlop J. S., Serjeant S., Peacock J. A., Ivison R. J., Oliver S., Mann R. G., Lawrence A., Efstathiou A., Rowan-Robinson M., Hughes D. H., Archibald E. N., Blain A., Longair M., 2002, MNRAS, 331, 817
- Silva L., Granato G. L., Bressan A., Danese L., 1998, ApJ, 509, 103
- Smail I., Chapman S. C., Blain A. W., Ivison R. J., 2004, ApJ, 616, 71
- Smail I., Ivison R. J., Blain A. W., 1997, ApJ, 490, L5
- Smail I., Ivison R. J., Blain A. W., Kneib J.-P., 2002, MNRAS, 331, 495
- Smail I., Ivison R. J., Kneib J.-P., Cowie L. L., Blain A. W., Barger A. J., Owen F. N., Morrison G., 1999, MNRAS, 308, 1061
- Swinbank A. M., Smail I., Chapman S. C., Blain A. W., Ivison R. J., Keel W. C., 2004, ApJ, 617, 64
- Takagi T., Arimoto N., Hanami H., 2003, MNRAS, 340, 813
- Takagi T., Hanami H., Arimoto N., 2004, MNRAS, 355, 424
- Takagi T., Pearson C. P., 2005, MNRAS, 357, 165
- Takagi T., Vansevicius V., Arimoto N., 2003, PASJ, 55, 385
- Thompson D., Beckwith S. V. W., Fockenbrock R., Fried J., Hippelein H., Huang J.-S., von Kuhlmann B., Leinert C., Meisenheimer K., Phleps S., Röser H.-J., Thommes E., Wolf C., 1999, ApJ, 523, 100
- van Dokkum P. G., Förster Schreiber N. M., Franx M., Daddi E., Illingworth G. D., Labbé I., Moorwood A., Rix H., Röttgering H., Rudnick G., van der Wel A., van der Werf P., van Starckenburg L., 2003, ApJ, 587, L83
- Wang W.-H., Cowie L. L., Barger A. J., 2006, ApJ, 647, 74
- Webb T. M. A., Brodwin M., Eales S., Lilly S. J., 2004, ApJ, 605, 645
- Webb T. M. A., Lilly S. J., Clements D. L., Eales S., Yun M., Brodwin M., Dunne L., Gear W. K., 2003, ApJ, 597, 680
- Webb T. M. A., van Dokkum P., Egami E., Fazio G., Franx M., Gawiser E., Herrera D., Huang J., Labbé I., Lira P., Marchesini D., Maza J., Quadri R., Rudnick G., van der Werf P., 2006, ApJ, 636, L17

APPENDIX A: ESTIMATE ON THE NUMBER OF CHANCE DETECTIONS IN OUR SCUBA MAPS

The large beam size of the JCMT (14.7'' FWHM at 850 μm) could lead to some chance detections of spurious $>3\sigma$ peaks at the position of NIR-selected galaxies. We statistically evaluate the expected number of $>3\sigma$ chance detections for a given class of galaxies as follows. The probability of randomly finding an object at $>3\sigma$ in the 850- μm map may be given by the ratio of the number of pixels with $>3\sigma$ to the total number of pixels in the region under consideration. For the SHADES/SIRIUS K_s -band area, we found this probability as $p(>3\sigma) = 0.45 \times 10^{-2}$ for the SHADES B-map and 0.85×10^{-2} for the D-map⁷. If we randomly distribute n objects in the 850- μm map, the number of objects spuriously detected with $>3\sigma$ would follow a Poisson distribution with the parameter of $\mu = np(>3\sigma)$. For 307 NIRGs, we derive $\mu = 1.4$ and 2.6 for the B- and D-map respectively, giving the mean number of $>3\sigma$ detections by chance. This means that we must confirm whether submm-detected NIRGs are

⁷ The difference in $p(>3\sigma)$ between the maps may be explained by the difference in the adopted pixel size.

Table 1. Statistics of NIR-selected galaxies (NIRGs)

Population	Area ^a K_s or J	Number	Surface density [arcmin ⁻²]
K_s -detected object	K_s	1308 (992) ^b	11.5
Star	K_s	95 (64)	0.83
NIRGs	J	307 (245)	3.14
ERO	K_s	249 (201)	2.18
DRG	J	84 (67)	1.09
ERO and non-DRG	J	105 (84)	1.36
DRG and non-ERO	J	38 (28)	0.49
ERO and DRG	J	46 (39)	0.60
BzK	K_s	168 (132)	1.47
BzK and ERO and non-DRG	J	17 (14)	0.22
BzK and DRG and non-ERO	J	14 (8)	0.18
BzK and ERO and DRG	J	19 (16)	0.25

a) Image (K_s - or J -band area) for which the number of objects are derived.

b) Total number of objects, with the number within the SHADES area given in parentheses.

Table 2. Submm properties of submm-bright NIR-selected galaxies

Source	Map ^a	S/N ^b	$\theta_{850\mu\text{m}}^c$ [arcsec]	$S_{850\mu\text{m}}^d$ [mJy]	$S_{24\mu\text{m}}$ [μJy]	$S_{1.4\text{GHz}}$ [μJy]	SHADES ID ^e [SXDF]
300	B,D	3.1	4.5	5.7 ± 2.1	546 ± 27	27.8 ± 7.0	850.30
445	B	3.3	2.9	5.6 ± 2.1	357 ± 24	$250. \pm 7.4$	850.27
912	B,D	4.1	2.1	4.4 ± 1.8	511 ± 27	$145. \pm 7.7$	850.4
1390	B,D	3.4	1.8	4.0 ± 2.8	446 ± 29	29.6 ± 7.5	(850.62) ^f
Unconfirmed detections							
718	B,D	3.3	2.3	4.0 ± 2.1	< 450	< 35	850.70
1133	D	3.0	6.6	3.0 ± 2.1	< 450	< 40	850.77

Notes: The upper limits correspond to 5σ . a) SHADES map in which NIRGs are detected

b) S/N at the position of NIRGs in the SHADES map. We adopt values from the SHADES B-map if NIRGs are detected in both B and D maps. c) The angular separation between submm and NIR position. Submm positions are taken from the SHADES source catalogue. For ID1390, we adopt the submm position from the SHADES B-map. d) Deboosted 850- μm flux densities from the SHADES source catalogue, using the algorithm of Coppin et al. (2005). e) Source names in the SHADES source catalogue. f) Source name from a preliminary SHADES source catalogue.

genuine submm emitters or not by other means. Here we require a detection at 24 μm or radio to identify submm-bright NIRGs, along with the detection in the SCUBA map. For example, only 15 NIRGs are found to be detected at 24 μm . This results in $\mu = 0.067$ and 0.13 for 24 μm -detected NIRGs in the B-map and D-map, respectively. Thus, we expect no chance detections in the SCUBA map if NIRGs are detected at 24 μm .

Table 3. Optical – NIR properties of submm-bright NIR-selected galaxies

Source	R.A. [J2000]	Dec. [J2000]	K_s	$R - K_s$	$J - K_s$ [AB mag]	$B - z'$	$z' - K_s$	Notes				
								BzK	ERO	DRG	$24\mu\text{m}$	Radio
300	2 17 40.01	-05 01 15.7	21.14	3.43	1.56	2.05	2.61	Y	Y	Y	Y	Y
445	2 18 07.92	-05 01 45.7	22.00	4.39	> 1.40	1.75	3.21	Y	Y	Y	Y	Y
912	2 17 38.67	-05 03 39.4	21.64	2.59	...	1.20	2.05	Y	N	...	Y	Y
1390	2 18 07.74	-05 06 10.5	21.13	3.67	2.02	2.52	2.56	(N) ^a	Y	Y	Y	Y

Notes: A ‘Y’ (‘N’) in the last five columns indicate that the galaxy is (not) BzK -selected galaxy, ERO, DRG, $24\mu\text{m}$ -detected and radio-detected. a) After the colour correction on $B - z$ and $z - K$, this source becomes a non- BzK -selected galaxy, as shown in Figure 7. This correction is adopted to match the observed colour sequence of stars to that of Daddi et al. (2004).

Table 4. Summary of stacking analysis at $850\mu\text{m}$

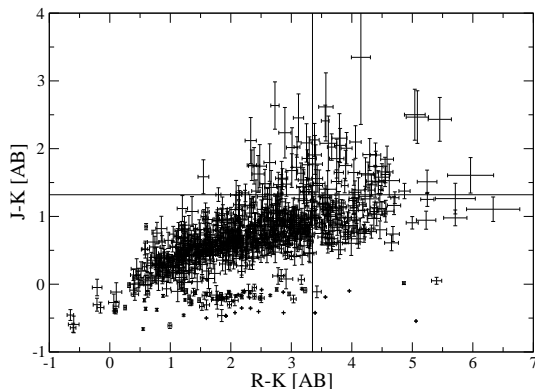
Class	Number ^a	$\langle S_{850\mu\text{m}} \rangle^b$ [mJy]	K-S Prob. ^c [%]	% Resolved flux ^d [%]	E.B.L. ^e [Jy deg ⁻²]
$BzKs$	112	0.52 ± 0.19	5.91	32 ± 18	3.8 ± 1.2
EROs	178	0.53 ± 0.16	1.70	18 ± 9	5.1 ± 1.5
DRGs	56	0.30 ± 0.28	45.91

a) The number of objects used for the stacking analysis. b) The average $850\mu\text{m}$ flux of non-detected objects, which are $> 7''$ away from individual sources. c) The probability from the Kolmogorov-Smirnov test. that the flux distribution of objects are derived from the same sample. d) The fraction of the flux density in individually detected sources. e) The extragalactic background light at $850\mu\text{m}$ from each class of objects.

Table 5. Summary of the SED fitting with the SBURT model

Source	χ^2/ν^a	z_{phot}	Age ^b [Gyr]	Θ^c	Ext. ^d	$\log M_{\text{star}}$ [M_{\odot}]	$\log M_{\text{gas}}$ [M_{\odot}]	$\log L_{\text{bol}}^e$ [L_{\odot}]	A_V [mag]	$\log \text{SFR}$ [$M_{\odot} \text{ yr}^{-1}$]	M_V^f [mag]	$(U - V)^f$ [mag]
300	0.91	2.8	0.2	2.0	SMC	10.8	10.7	12.7	1.3	2.7	-20.1	1.3
445	1.47	2.1	0.5	1.0	LMC	10.9	10.0	12.1	2.3	2.0	-20.3	1.5
912	0.47	2.4	0.07	1.4	LMC	10.7	11.1	13.1	3.1	3.2	-20.1	0.9
1390	2.45	2.4	0.4	1.4	LMC	11.1	10.4	12.5	1.5	2.4	-20.7	1.4
$\langle BzKs \rangle^g$...	1.9^h	0.4	1.6	LMC	10.6	9.8	11.9	1.1	1.8	-19.4	1.4

a) χ^2 divided by the degree of freedom ν . b) Starburst age with the evolutionary time scale of $t_0 = 0.1 \text{ Gyr}$. c) Compactness parameter of starburst region. d) Extinction curve used. e) Bolometric luminosity. f) Predicted present-day V -band magnitude and $U - V$ (Vega), assuming the passive evolution after the observed epoch. g) Model parameters for an average SED of submm-faint $BzKs$ with $1.5 < (B - z) < 2.5$ h) Assumed redshift for the SED fitting.


Figure 1. $J - K_s$ versus $R - K_s$ for K_s -band detected objects in the SIRIUS J -band area. The selection criteria for EROs and DRGs are indicated with a vertical line and a horizontal line, respectively.

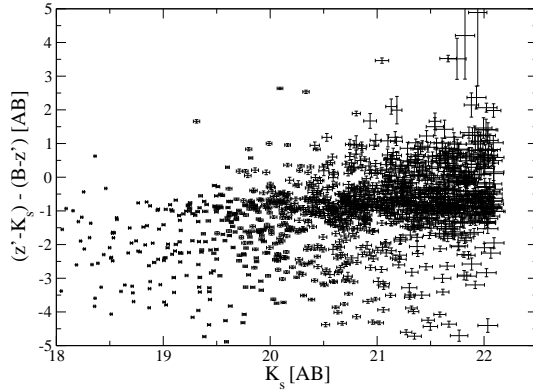


Figure 2. BzK colour vs. K_s magnitude for K_s -band detected objects. Here the $z' - K_s$ and $B - z'$ colours have *not* been colour-corrected in order to show the original photometric errors. The BzK selection criterion proposed by Daddi et al. (2004) corresponds to $(z' - K_s) - (B - z') = 0.2$ for the adopted colour correction (see text).

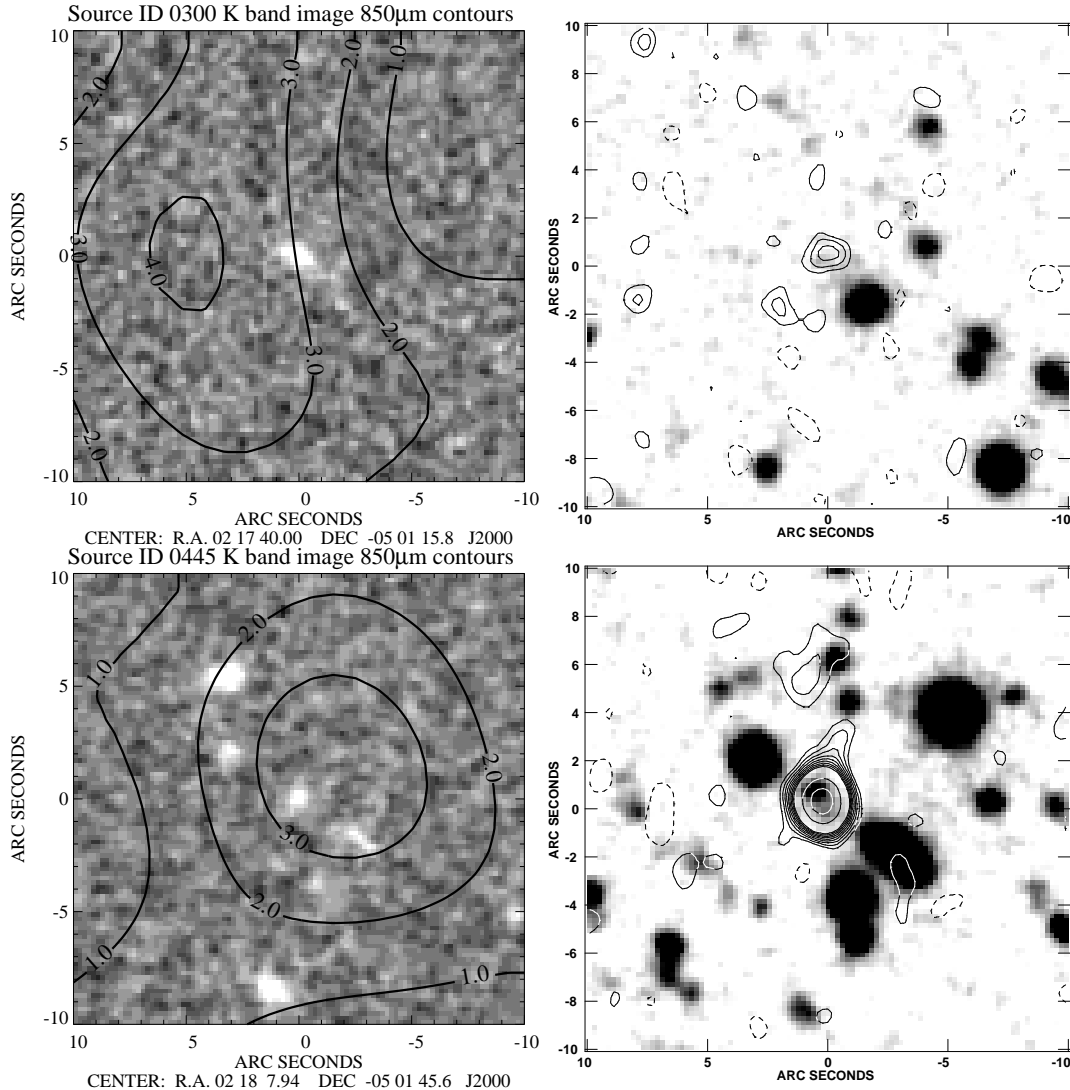


Figure 3. [Left column] Contours of SCUBA $850\text{-}\mu\text{m}$ for submm-bright NIR-selected galaxies. The corresponding S/N ratios at $850\text{ }\mu\text{m}$ are indicated at each contour line. The underlying images are K_s -band with $20''$ on a side. The names of the sources are indicated at the top of each image. [Right column] Contour maps of radio (1.4 GHz) on negative images at R -band for the same regions as shown in the left panels. Contour lines are shown at $-2, 2, 3, 4, \dots, 10, 20, \dots, 100 \times \sigma$. Positive (negative) contours are indicated with solid (dashed) lines.

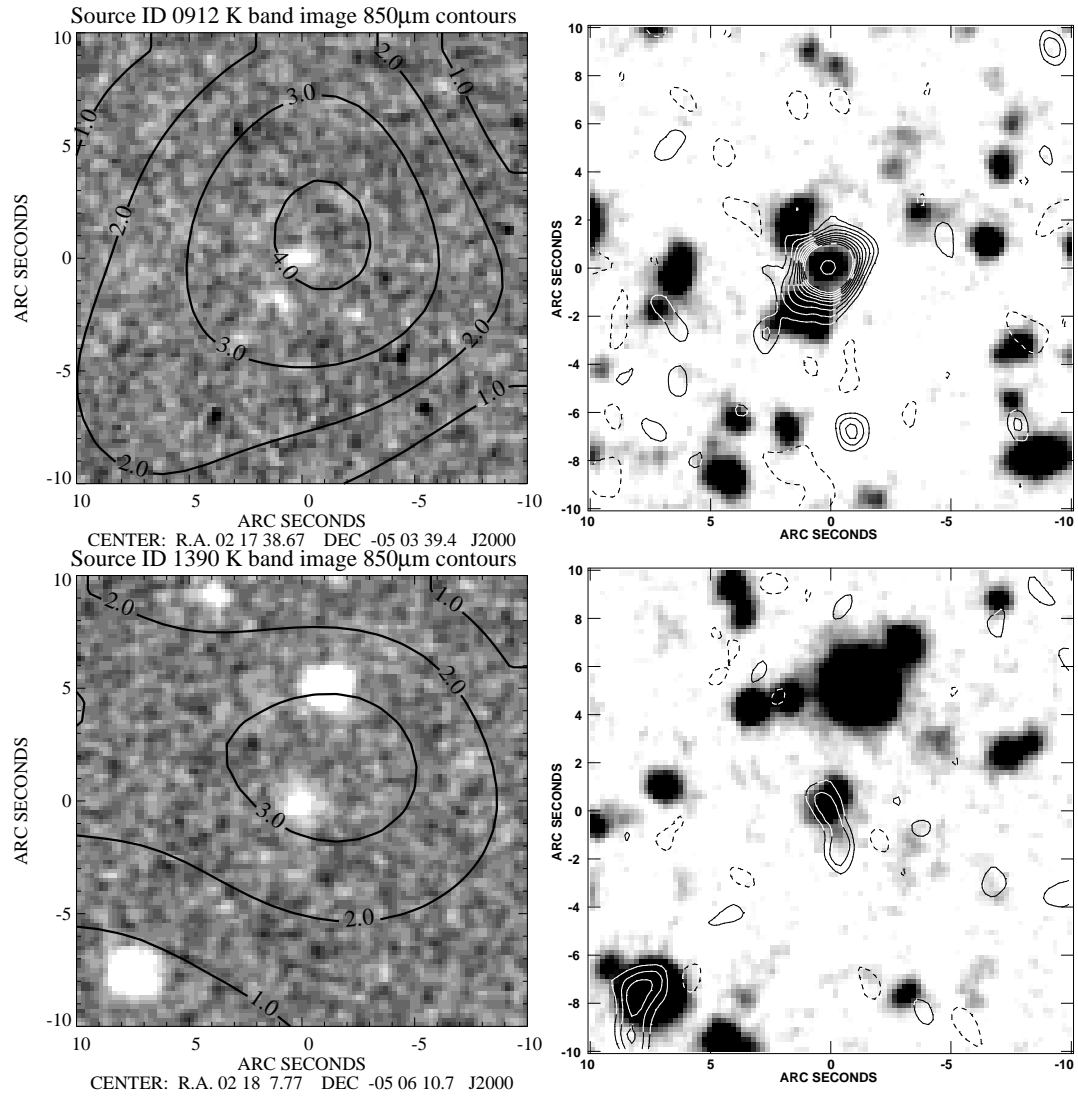


Figure 3. - continued.

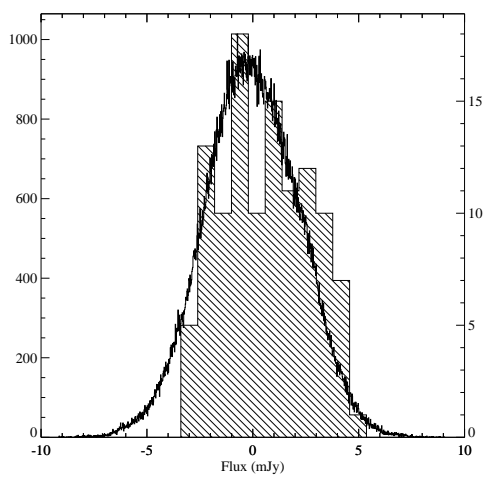


Figure 4. Histograms of the 850- μ m flux at the position of *BzKs* (shaded; right axis), compared to the histograms for the unmasked regions of the SCUBA map as a whole (open; left axis).

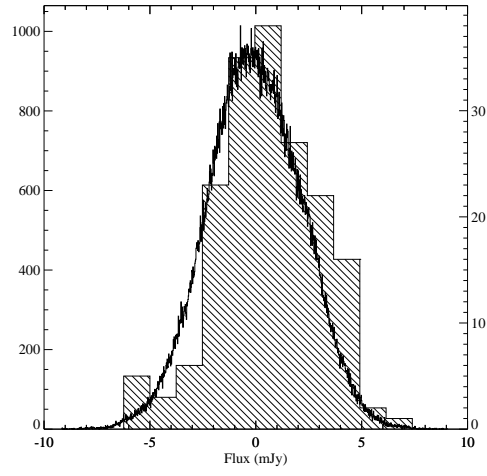


Figure 5. Same as Figure 4, but for EROs.

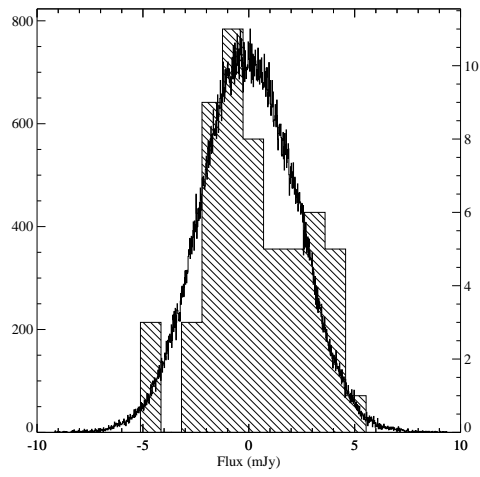


Figure 6. Same as Figure 4, but for DRGs.

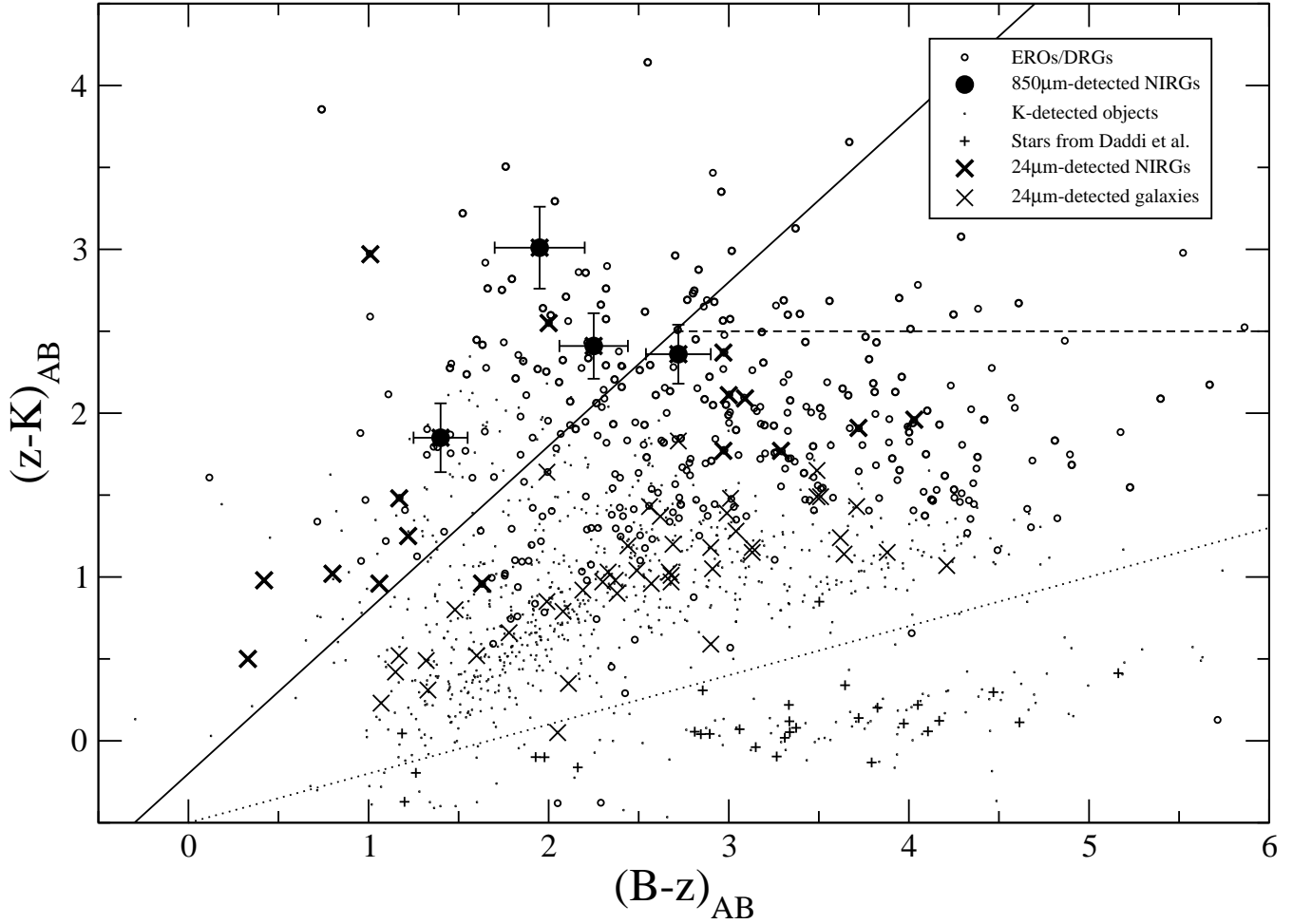


Figure 7. The BzK diagram for K_s -detected sources in the SXDF/SIRIUS field. Solid circles indicate submm-bright NIRGs. The photometric errors include those of colour corrections on $B - z$ and $z - K$. Both EROs and DRGs are indicated with small circles. Large thick/thin crosses are for NIR-selected/ K_s -detected galaxies which are detected at $24\mu\text{m}$ with SWIRE. Small pluses indicate stars from Daddi's catalogue. We depict the BzK -selection criterion with a solid line. Dashed and dotted lines are boundaries for selecting passively evolving galaxies and stars, respectively.

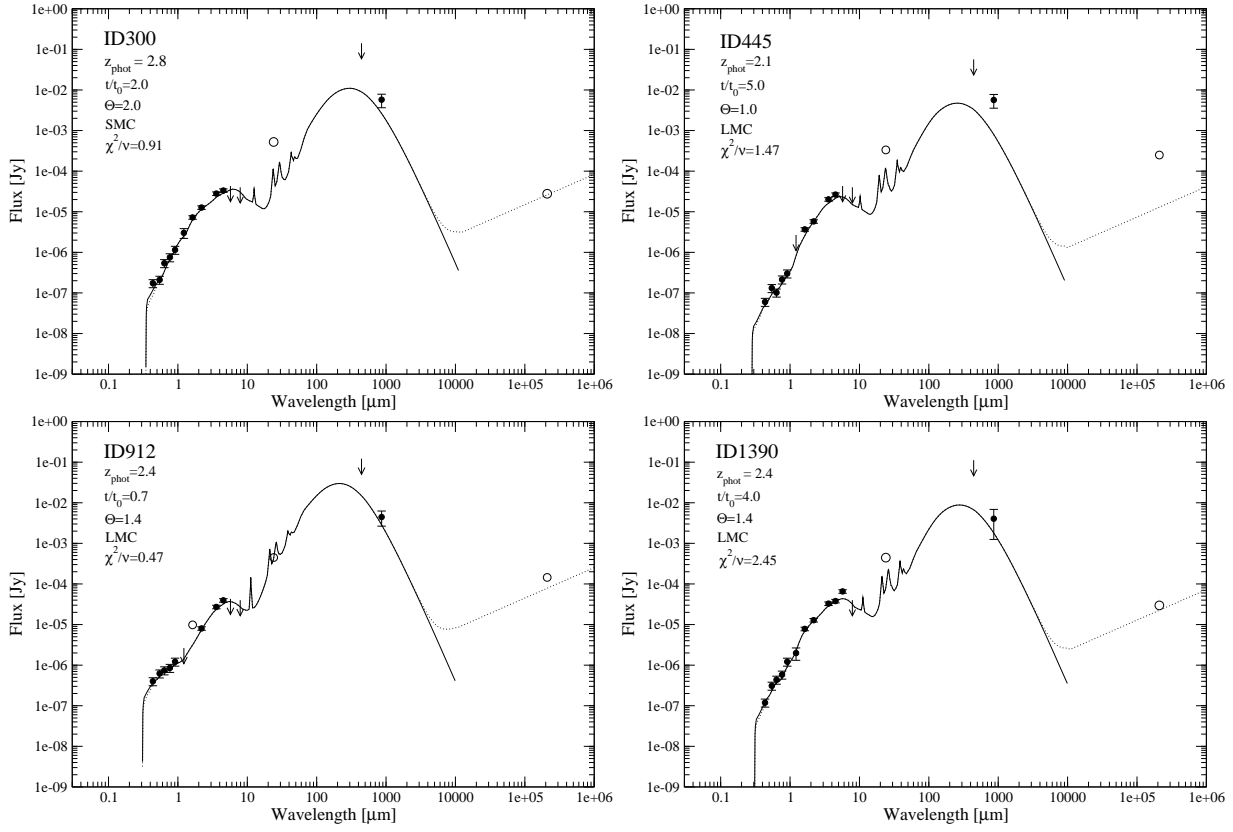


Figure 8. Solid and dotted lines indicate the best-fitting SBURT model without and with an extended radio component of the SED, respectively. The data points used for the SED fitting are shown as solid circles. Arrows indicate the 5σ upper limits. See Section 6.2.1 for the definition of the fitting parameters.

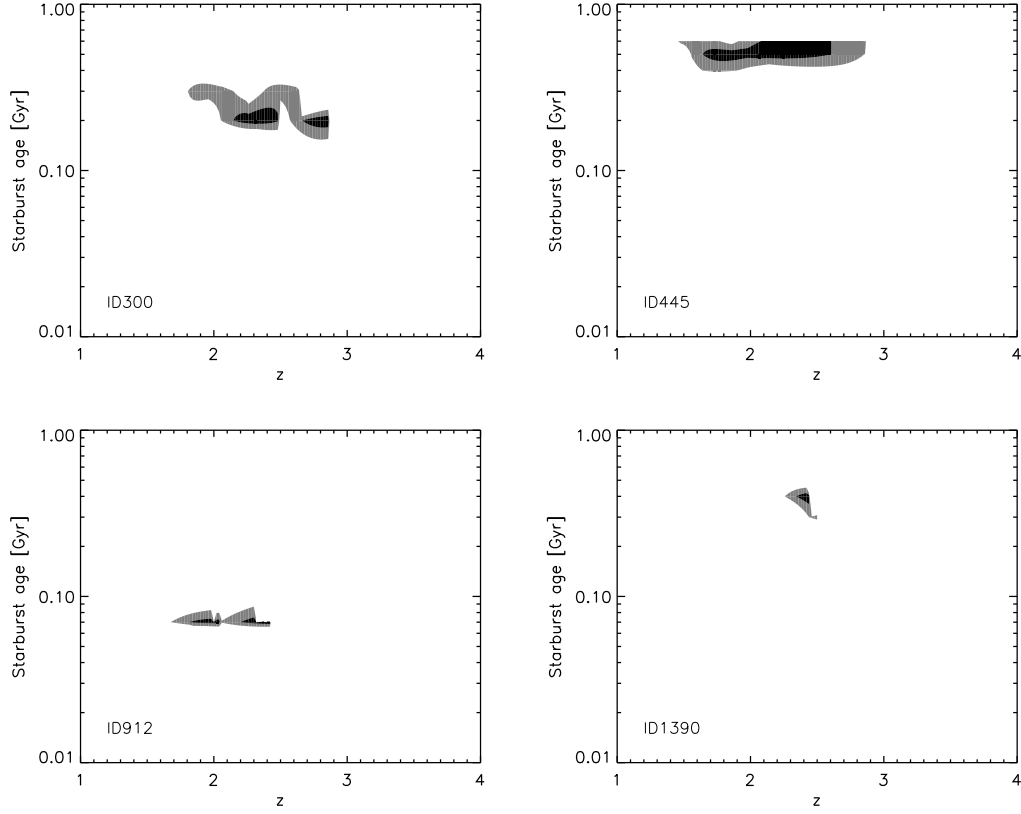


Figure 9. Contour maps of $\Delta\chi^2$ from the SED fitting in a plane of starburst age (with $t_0 = 0.1$ Gyr) and redshift. The contours are depicted at $\Delta\chi^2 = 2.71, 6.63$, having the probabilities of 90 and 99 % when projected on to each axis. We note that there are no local minima at $z < 1$ and $z > 4$.

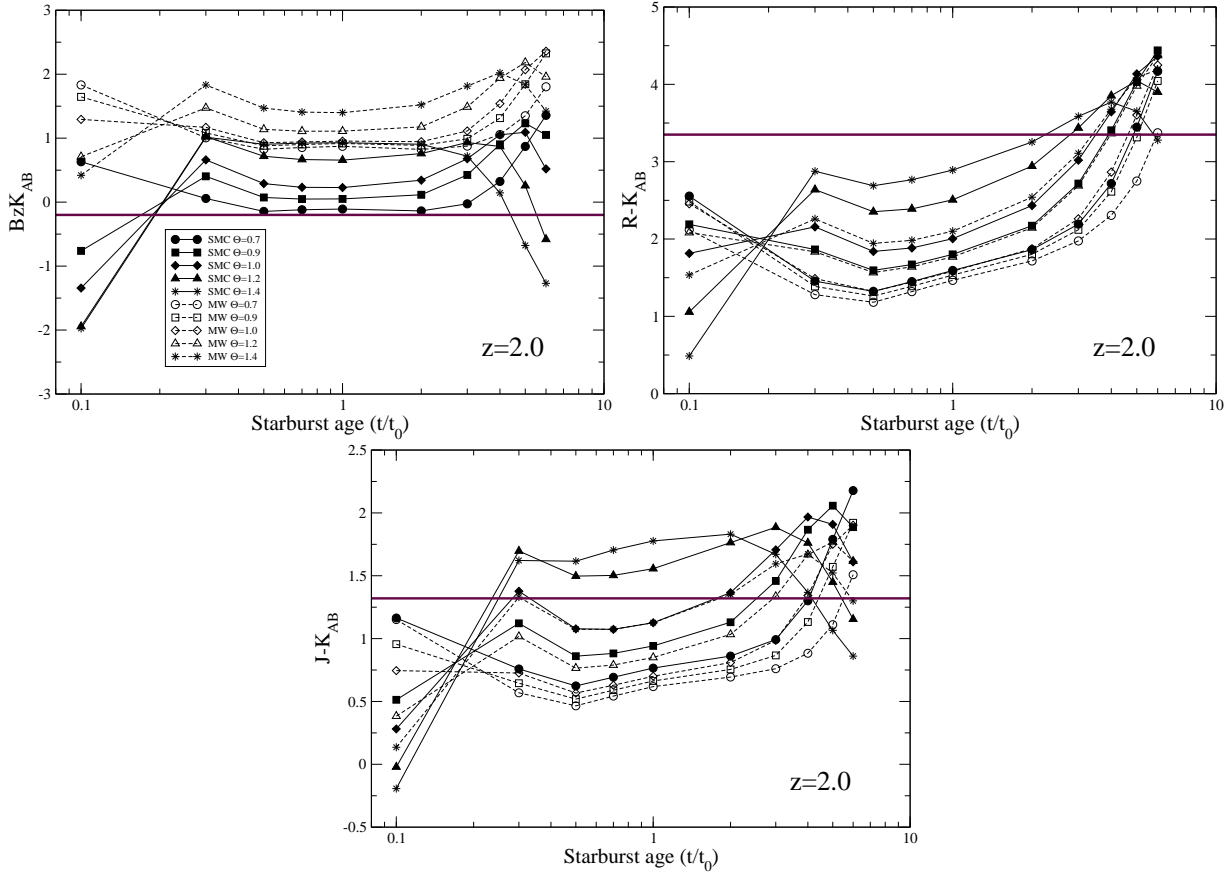


Figure 10. BzK , $R-K$ and $J-K$ colours of the SBURT model at $z = 2$ as a function of starburst age, which show the range of model parameters to satisfy BzK , DRG, and ERO selection criteria. Model parameters for a given line symbol are shown in the legend box. Horizontal lines indicate the colour boundary for $BzKs$, DRGs and EROs.

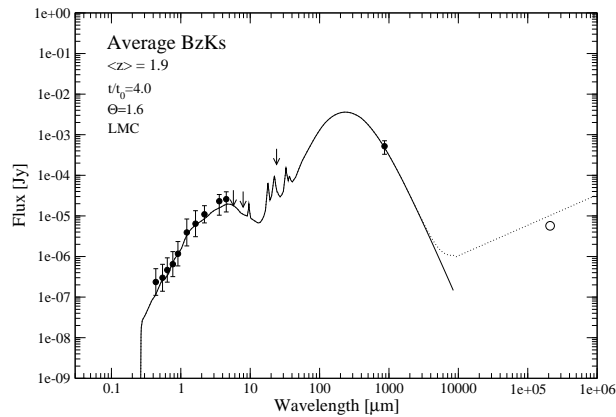


Figure 11. Average SED of $BzKs$ with $1.5 < (B - z') < 2.5$ and a representative SBURT model for the average SED. Symbols are the same as in Figure 8.